Brain orchestra under spontaneous conditions: Identifying communication modules from the functional architecture of area V1

Maria Papadopouli[1,2*], Ioannis Smyrnakis[3], Emmanouil Koniotakis[2], Mario-Alexios Savaglio[1,2], Christina Brozi[1,2], Eleftheria Psilou[1,2], Ganna Palagina[4], Stelios Manolis Smirnakis[4]

[1]Department of Computer Science, University of Crete, Heraklion, Greece.
[2]Institute of Computer Science, Foundation for Research & Technology-Hellas, Heraklion, Greece.
[3]Hellenic Mediterranean University, Heraklion, Greece.
[4]Department of Neurology, Brigham and Women's Hospital, Harvard Medical School, Boston, USA.

*Corresponding author(s). E-mail(s): maria@csd.uoc.gr;

We used two-photon imaging to record from granular and supragranular layers in mouse primary visual cortex (V1) under spontaneous conditions and applied an extension of the spike time tiling coefficient (STTC; introduced by Cutts and Eglen) to map functional connectivity architecture within and across layers. We made several observations: Approximately, 19-34% of neuronal pairs within 300 μm of each other exhibit statistically significant functional connections, compared to $\sim$10% at distances of 1mm or more. As expected, neuronal pairs with similar tuning functions exhibit a significant, though relatively small, increase in the fraction of functional inter-neuronal correlations. In contrast, internal state as reflected by pupillary diameter or aggregate neuronal activity appears to play a much stronger role in determining inter-neuronal correlation distributions and topography. Overall, inter-neuronal correlations appear to be slightly more prominent in L4. The first-order functionally connected (i.e., direct) neighbors of neurons determine the hub structure of the V1 microcircuit. L4 exhibits a nearly flat degree of connectivity distribution, extending to higher values than seen in supragranular layers, whose distribution drops exponentially. In all layers, functional connectivity exhibits small-world characteristics and network robustness. The probability of firing of L2/3 pyramidal neurons can be predicted as a function of the aggregate activity in their first-order functionally connected partners within L4, which represent their putative input group. The functional form of this prediction conforms well to a ReLU function, reaching up to firing probability one in some neurons. Interestingly, the properties of L2/3 pyramidal neurons differ based on the size of their L4 functional connectivity group. Specifically, L2/3 neurons with small layer-4 degrees of connectivity appear to be more sensitive to the firing of their L4 functional connectivity partners, suggesting they may be more effective at transmitting synchronous activity downstream from L4. They also appear to fire largely independently from each other, compared to neurons with high layer-4 degrees of connectivity, and are less modulated by changes in pupil size and aggregate population dynamics. Information transmission is best viewed as occurring from neuronal ensembles in L4 to neuronal ensembles in L2/3. Under spontaneous conditions, we were able to identify such candidate neuronal ensembles, which exhibit high sensitivity, precision, and specificity for L4 to L2/3 information transmission. In sum, functional connectivity analysis under spontaneous activity conditions reveals a modular neuronal ensemble architecture within and across granular and supragranular layers of mouse primary visual cortex. Furthermore, modules with different degrees of connectivity appear to obey different rules of engagement and communication across the V1 columnar circuit.

1 Introduction

Neuronal ensembles are crucial to information encoding. Much has been learned about the computational properties of single neurons. However, we remain far from understanding how networks of cortical cells coordinate and interact with each other to process information. Several pioneering works have proposed theories regarding how the configuration of neuronal ensembles encodes information in the cortex[1–6]. Within these ensembles sets of coactive neurons, demonstrate synchronous or more generally, spatiotemporally correlated activity under both spontaneous and evoked activity conditions[2,7–11]. Nevertheless, how groups of neurons coordinate with each other to parse and process information remains poorly understood. Here we focus on employing functional connectivity analysis to identify neuronal ensembles that fire in *synchrony* under *spontaneous* conditions. Ensembles of neurons that fire in synchrony are likely to be more efficient at relaying shared information to downstream targets[12] as well as more likely to belong to networks of neurons subserving similar functions.

Spontaneous patterns of activity reflect the intrinsic dynamics of the brain in the absence of external stimulation or task performance. Under these conditions, pairwise functional connectivity, a measure of synchrony across pairs of neurons, is shaped directly or indirectly by anatomical connectivity. Functional connectivity analysis can therefore reveal the architecture of ensembles of neurons that share paths of anatomical connectivity between each other. Activity patterns generated across such neuronal ensembles represent, in a sense, a "vocabulary space" that is the currency of information processing in the cortex. It has been further suggested that the "pattern vocabulary space" spanned by spontaneous patterns of activity is shared with population activity patterns elicited during sensory responses[13–15]. This rather strong interpretation remains a matter of debate. Be that as it may, here we focus on studying the structure of spontaneous activity in the primary visual cortex in its own right, in order to understand how patterns of activity are organized and processed across granular and supragranular layers in the absence of visual stimulation. We expect that in the absence of sensory input, behavioral parameters reflecting the animal's internal state will likely provide the dominant factor behind the modulation of spontaneous patterns of activity and may influence strongly the topographical layout of functional connectivity. Below, we aim to help address several questions that, to the best of our knowledge, still remain unresolved in the literature: **1)** What is the architecture of functionally connected neuronal ensembles in different layers of mouse area V1 and how does it depend on the duration of the experimental data used to compute it? **2)** What does the "pattern vocabulary space" observed under spontaneous activity conditions look like, and **3)** how are firing patterns relayed from granular to supragranular layers via neuronal ensemble to ensemble transmission? **4)** How do behavioral parameters reflecting the internal state modulate these cortical activity processing streams?

To address these questions, we employed large field mesoscopic 2-photon calcium imaging to record essentially simultaneously spontaneous neuronal activity from thousands of pyramidal neurons in three cortical planes, corresponding to cortical laminae 2, 3 and 4. Although the imaged field of view extended beyond area V1, here we focus solely on the analysis of data from the primary visual cortex. Functional connectivity was formed based on an extension of the spike time tiling coefficient (STTC), a measure shown by Eglen and Cutts to be superior to other correlation measures[16]. Encouragingly, our results remain robust to a change of correlation measure to the Pearson correlation coefficient. Despite the relatively low temporal resolution of calcium dyes and frame duration of 155ms we adopted here, it was feasible to obtain a rich and reliable set of functional connectivity measurements across the cortical circuitry examined.

Our approach here represents a step beyond single units to uncover principles of multi-neuronal ensemble activity generation and propagation in the neocortex. The study of first-order functional connectivity groups identified under spontaneous activity allowed us to identify organizational modules within area V1, consisting of groups of neurons that fire in synchrony more than expected by chance. In what follows, we present evidence arguing that these modules contain clues about the operations executed by the V1 cortical networks, and how these are modulated by fluctuations in the animal's behavioral state.

To our knowledge, our work represents the first time that functional connectivity analysis is employed to analyze cortical columnar processing at the microcircuit level. It is worth noting that in other, lower resolution, contexts, functional connectivity analysis has proven valuable for shedding light on the mechanisms of information processing and integration across brain areas, while anomalous patterns of functional connectivity have been linked to neurological and psychiatric disorders[17,18]. We expect that functional connectivity analysis at the level of the cortical microcircuit will yield similarly important information about cortical circuit function and dysfunction in the future.

2 Results

Experiments, data collection, and pre-processing

Five adult mice (10-12 weeks of age), expressing GCaMP6s in pyramidal neurons as the F1 cross between BL6-SLC17a7-Cre X Ai162 (JAX stocks 023527 and 031562), underwent mesoscopic two-photon imaging covering the majority of dorsal area V1 and nearby extrastriate cortex (areas V1, LM, RL, AL; Fig. 1) while being head-posted on a treadmill in quiet wakefulness. Periods of spontaneous walking were few and when excluded from the analysis, the main trends remained the same (see Suppl. Figures 11.1 and 11.2). Imaging was performed at least 2 weeks following craniotomy to ensure inflammation had subsided. Images were acquired at 6Hz over a $\sim$1.2 x 1.2 mm^2 field of view (Fig. 1D) sampling simultaneously across 4 planes corresponding to V1 layers 2 (80-210μm), 3 (285-330μm), 4 (350-400μm), and 5 (500 to 800 μm) (Fig. 1A). Here we report on the analysis of data from the granular (L4) and supragranular (L2/3) layers. Images were pre-processed for motion correction and underwent automatic segmentation and deconvolution using the CNMF CaImAn algorithm[19]. The deconvolved signal was thresholded (see methods) to yield calcium "eventograms" that were analyzed. The results reported below were robust to the choice of threshold (see Suppl. Fig. 1.1). In what follows, we use the threshold yielding calcium event rates closest to the firing rates reported in the literature[20] (Fig. 1E). Neurons with event rates less than 0.01Hz (0.27% of the 4187 neurons that were segmented per mouse on average in area V1) were excluded from the analysis. Neurons located less than 15μm from the periphery of the field of view were also excluded in order to avoid potential edge effects arising from incomplete correction of motion artifacts. Overall, 7.76% of area V1 neurons recorded across all mice were excluded from the analysis.

Identifying significant pairwise inter-neuronal functional connections

To quantify functional connectivity, we used the spike time tiling coefficient (STTC), which performs favorably against 33 other commonly-used measures and is less sensitive to firing rate (see methods). STTC is a function of the temporal window (Δt) over which synchrony is defined and is both symmetrized and normalized to lie within [-1, 1]. The bulk of results presented below report STTC values computed for Δt=0, corresponding to neurons that fire in synchrony within one calcium imaging frame. In our experiments imaging frames are $\sim$155ms long, so the temporal correlations we can compute are insensitive to temporal differences smaller than 155ms.

To determine whether there is a statistically significant functional connection between two neurons, their STTC was compared to a null distribution of STTC values calculated by randomly reshuffling their calcium eventogram time series 500 times (Fig. 2, gray histogram), yielding a z-score that determines the level of significance. Figs. 2A, D histogram all pairwise STTC values in L4 (green) and 2/3 (blue), respectively. Note that the tails of the STTC distributions extend beyond the null (gray) histograms both in the positive (correlated) and negative (anti-correlated) directions, although the skew is considerably stronger toward positive STTC values. Figures 2B, E, and H plot only highly significant positive correlations (corresponding to z-score$>$ 4); Magnified insets show the relatively diminutive tail of the null distribution. Figure 2G illustrates the percentage of neuronal pairs with significant positive functional connections as a function of the z-score threshold. Suppl. Fig. 2.7 shows the negative functional connectivity.

Area V1 contains a large fraction of significant but weak functional connections

At a conservative threshold of z-score$>$4, approximately 25% of neuronal pairs in L4 exhibit significant functional correlations compared to 14% in L2/3. In general, a larger fraction of neuronal pairs have positive functional connections in L4 compared to L2/3, consistent with the sparse firing patterns observed in supergranular layers[22]. As expected, significance (z-score) is strongly correlated with STTC strength (Suppl. Figure 2.4). Despite this, it should be noted that, although pairwise neuronal correlations can reach high statistical significance, they remain relatively weak. The vast majority of positive correlations have STTC values well below 0.2 (Figs. 2A, D, 3D), while the magnitude of negative correlations generally remains below (0.05) (Suppl. Fig. 2.7). Overall, our findings suggest that, in agreement with[23–26], there is a significant correlation architecture in area V1, even though on average the inter-neuronal correlation strength remains low (mean inter-neuronal STTC strength in L4 0.018 vs. 0.01 in L2/3; Figs. 2A, D) in agreement with Ecker *et al.*[27].

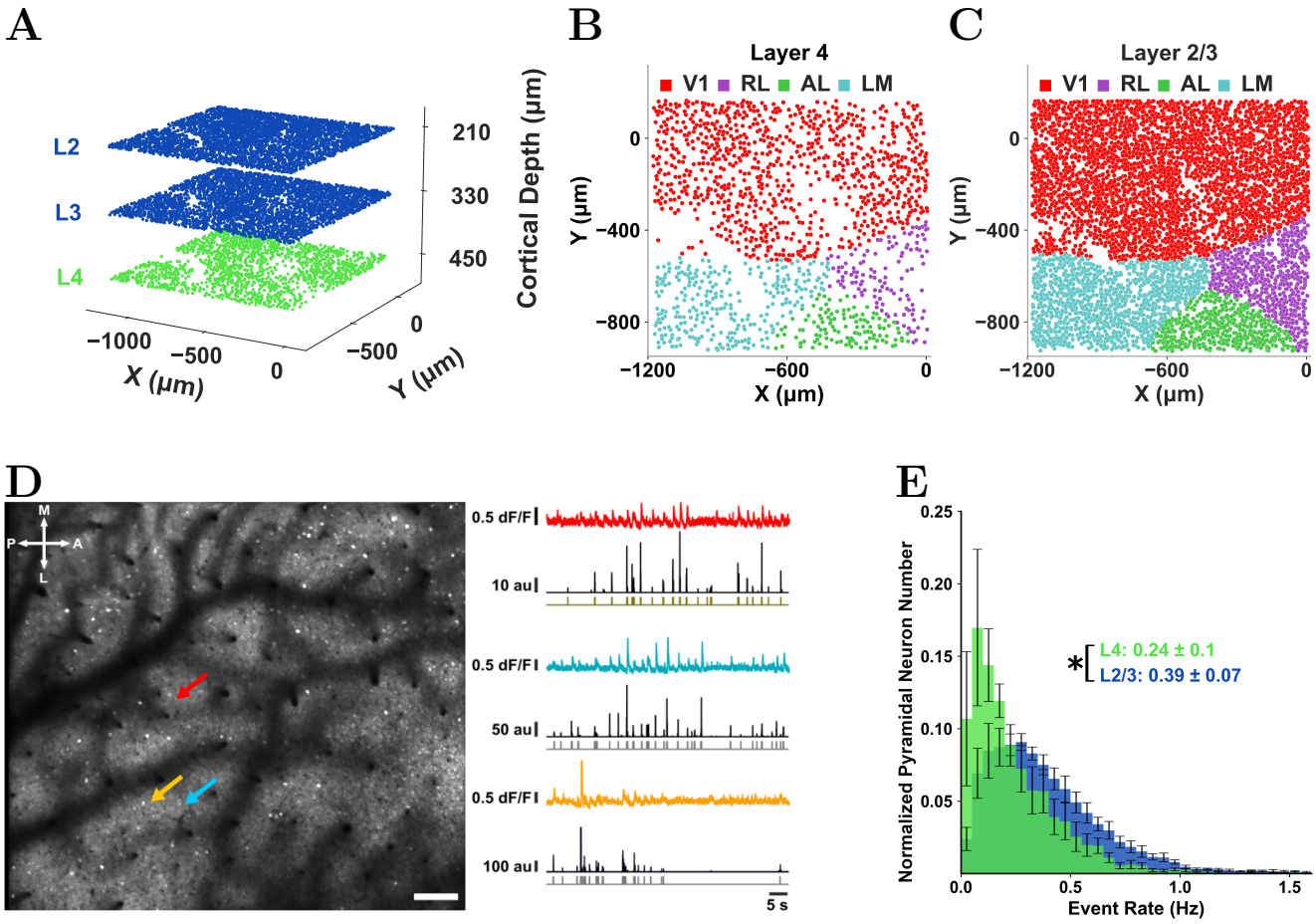

Fig. 1: Imaging Paradigm. A) Illustration of L4, L2, L3 fields of view (FOVs) simultaneously acquired at 6Hz. L2/3: blue. L4: green. B) Retinotopic map of the FOV acquired in layer 4. C) Retinotopic map of the FOV acquired in layer 2/3. D) Example FOV acquired in layer 2/3 at depth 210 µm. A: anterior, L: lateral, P: posterior, M: medial. Bar = 75 μm. Color arrows indicate 3 example cell bodies whose traces are shown in color on the right. Deconvolved firing probability traces shown in black below were obtained using the CaImAn algorithm[21] dF/F: fractional fluorescence change. au: the relative probability of firing in arbitrary units. Gray traces in the bottom represent the thresholded, binarized, probability that specific imaging frames contain a calcium event (0: no event; 1: event). E) Pyramidal neuron event rate histogram across animals. For each bin, the ratio of neurons with event rates belonging in that bin over all neurons in the corresponding layer is computed. Results are then averaged across animals (n=5). The results reported below are not sensitive to the threshold chosen. Error bars represent the standard error of the mean across animals (n=5). Inset: Mean event rate ± their standard deviation across animals (n=5), for each layer. P-values: "*"< 0.05; "**"< 0.01; and "***"< 0.001. The highest p-value obtained from the permutation of means, the Welch's t-test, and the ANOVA F-test is reported.

Existence of stronger "core" functional connectivity subnetworks

One might wonder how STTC significance and strength depend on the duration of the available recording. Functional correlations presented above were computed based on the entire duration of spontaneous activity recorded, i.e., 60 minutes. In general, longer recording duration yields a greater number of statistically significant connections whose strength progressively decreases, as weaker correlations between neurons rise to significance. The time dependence of the correlation analysis is illustrated in Suppl. Fig. 2.2. A plateau in the mean STTC weight begins to be approached but is not yet reached following 60 minutes of recording. It is interesting to ask which edges (i.e., statistically significant functional connections) remain robust across time. To take a stab at this question, we split

the one-hour recording into 15-minute long non-overlapping intervals and asked what percentage of edges identified within each interval remain significant across all other intervals. Only about 12% of edges persist across all four intervals (see Suppl. Figure 2.5), irrespective of cortical layer. These edges exhibit higher correlation strength, tend to connect neurons with higher similarity in their tuning function, and are typically shorter than edges computed across the entire 60-minute period (Suppl. Fig. 4.6). Similar trends are obtained when the analysis considers 15-minute non-overlapping intervals of *randomly selected frames* (see Suppl. Fig. 4.7). We suggest that these edges may form a core functionally connected network, that is a subnetwork of the larger network constructed based on the entire 60-minute recording period. It is interesting to speculate about the implications this has on the degree of flexibility of different functional connections and how the overall functional architecture may be modified in different behavioral states or with learning.

Dependence of Functional Connectivity on Distance

Figs. 2C and 2F plot the number of significant positive functional connections a neuron forms as a function of distance from its soma, expressed as a fraction of all possible pairwise correlations at that distance. Not surprisingly, significant positive functional connections form more densely with neighboring neurons[28–30], within ∼300μm from the cell body. However, the fraction of significant correlations exhibits a tail that extends a considerable distance and is slightly more prominent in L4 compared to L2/3. On average, at distances ∼1mm the fraction of significant positive functional connections is approximately 15% in L4 versus 7% in L2/3. However, the distribution has a long tail, decreasing with a distance slightly slower in L4 versus L2/3. Since the size of area V1 in the mouse is on the order of 2mm this implies that, unlike in primates, mouse area V1 pyramidal neurons can participate directly in computations that extend over a large area of the visual field. Interestingly, although by 1mm the fraction of significant correlations drops by ∼67% in L4 and ∼81% in L2/3, the average strength of these correlations remains comparatively stable with distance, decreasing only by 18% in L4 and 14% in L2/3, respectively (see suppl. Fig. 2.6). Thus, functional connectivity strength is not strongly dependent on distance, consistent to other work[31]. Interestingly, although physiological studies[31] find a minority of connections to be exceptionally strong among cortical pairs of neurons, these connections do not appear to be enough to drive a significant increase in functional connectivity strength, which remains universally weak and nearly uniform with distance across all neuronal pairs tested. Interestingly, the distribution of negative inter-neuronal correlations with distance differs from that of positive correlations. Overall compared to positively correlated edges, *anticorrelated ones appear to be more spread out, their distribution peaking on average at larger distances* (Suppl. Fig. 2.8 A,C). Specifically, while the fraction of positive correlations peaks close to the pyramidal neuron soma (Fig. 2C,F), the fraction of significantly anticorrelated connections peaks at a distance of approximately 600μm (Suppl. Fig. 2.8 A, C). Similarly to positively correlated functional connectivity (STTC) weights, negative STTC values also remain relatively stable as a function of distance, at least up to distances on the order of 1mm (Suppl. Fig. 2.8 B).

In sum, functional connectivity strength between pairs of pyramidal neurons remains weak in neocortex, consistent with Ecker *et al.*[32]. Nevertheless, both negative and positive statistically significant functional correlations exist in relative abundance and extend across considerable distances in area V1. These have a characteristic topography, with negative correlations peaking further away from the soma than positive correlations. This suggests that pyramidal neurons form functionally connected neighborhoods with a center surround arrangement of excitatory (denser at the center) versus inhibitory (denser at the surround) connectivity.

Relation of Functional Connectivity under Spontaneous Conditions to Tuning Properties

It is known that neurons with similar tuning functions tend to preferentially connect with each other[29,33,34]. However, noise correlations between pairs of neurons do not appear to depend strongly on orientation preference or, more generally, on tuning function similarity[32,35,36]. A natural question for us here was then to ask the degree to which neurons with similar tuning functions exhibit increased functional connectivity under spontaneous conditions. Neuronal orientation and direction tuning was estimated as in[37] using data obtained from the same neurons under the directional motion visual stimulation paradigm described in Fahey *et al.*[37] (see Methods).

Figure 3A histograms the preferred orientation of neurons in L2/3 and L4, showing, as expected, a cardinal axes preference in the mouse. Fig. 3B illustrates the excess probability with which pairs of neurons that have significant functional connections (z-score>4) belong to particular "orientation-preference difference" bins. This is expressed as a percentage of expected, derived from a control (null) distribution consisting of pairs that are not

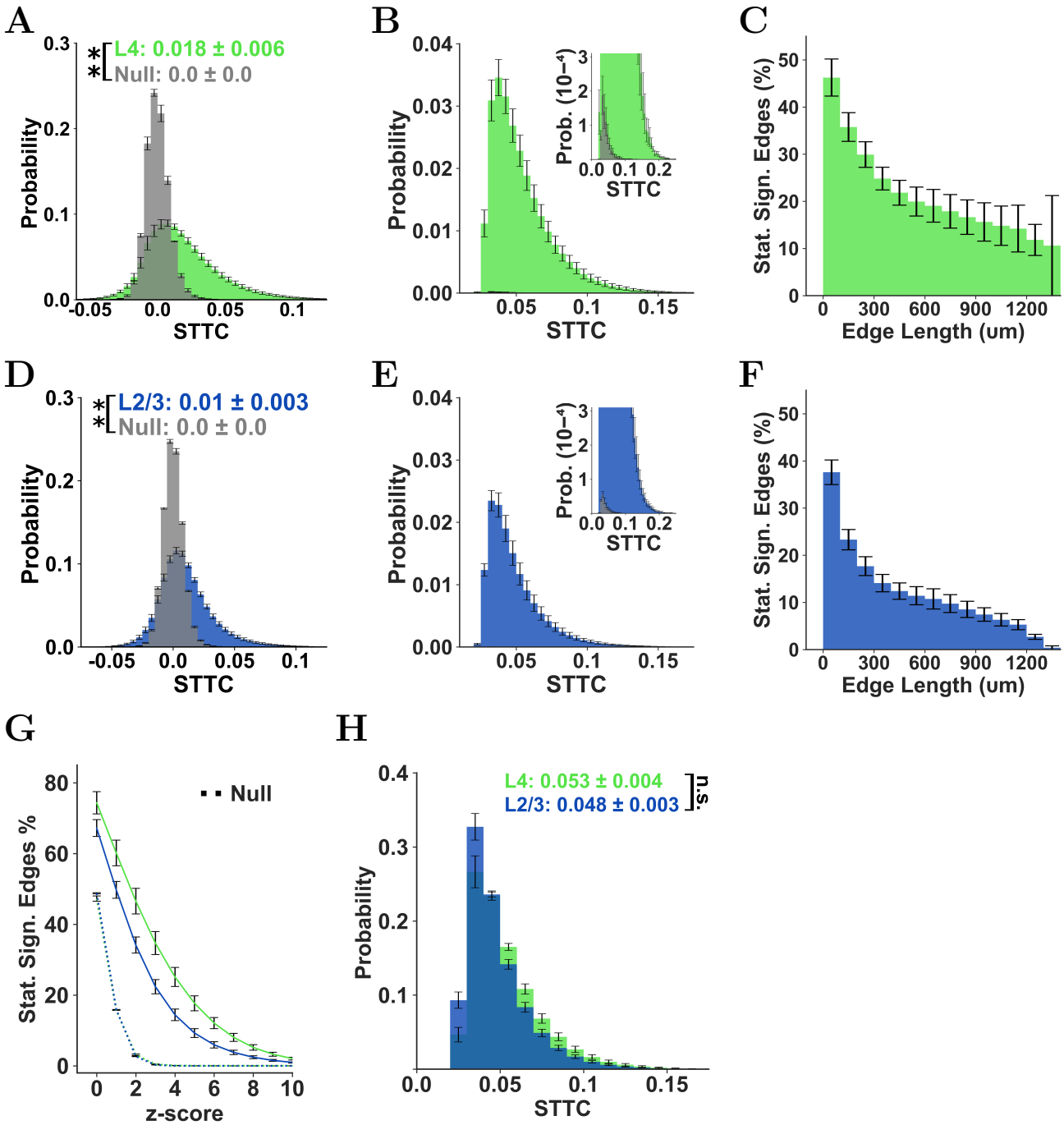

Fig. 2: Intra-layer Pairwise Functional Connectivity. A,D) Histograms of STTC values between pairs of neurons in layer 4 (A; green) versus layer 2/3 (D; blue). Gray: corresponding null distributions obtained by random circular shuffling. B,E) STTC histogram values with z-score > 4 in L4 (B; green) vs L2/3 (E; blue). The tails of the corresponding null distributions are visible only in the zoomed-in insets. C) Positive inter-neuronal functional correlations with z-score >4 ("edges") in L4 (green) as a function of distance from the soma, expressed as a fraction of total possible pairwise connections at that distance plotted in bins of 100μm. The histogram reflects the mean and error bars the standard error of the mean across animals. F) Similar to C for L2/3 (blue). Note that the fraction of significant functional connections drops with a distance slower in layer 4 than in layer 2/3. For example, the reduction in the fraction of significant functional connections within distance range [0,100] μm versus (100, 200] μm is more pronounced in L2/3 compared to L4 (right-tailed two-sample t-test, p-value: 0.001 across n=5 animals). Distance is measured on the X-Y plane, among pairs of neurons in the same layer (i.e., correlations here are computed separate for L2 and L3 and then plotted together). G) Percentage of significant pairwise STTC

Fig. 2: values as a function of the z-score threshold for L4 (green line) and L2/3 (blue line). L4 exhibits a greater percentage of significant STTC values at any given threshold compared to L2/3. Plots in either layer far exceed the expected null distributions (dotted lines). H) Histogram of STTC weights for all observed statistically significant edges (z-score > 4). Pairwise STTC correlation strength remains weak and distributed similarly across different layers. Histogram insets report the mean ± standard deviation of the sample means across mice (n=5), while error bars correspond to the standard error of the mean (SEM) across mice (n=5). P-values: "*" < 0.05; "**" < 0.01; and "***" < 0.001. The highest p-value obtained from the permutation of means, the Welch's t-test, and the ANOVA F-test is reported.

---

functionally connected (-2<z-score< 2). Evidently, functionally connected neurons have a higher probability to have similar orientation preference in all layers, though this tendency is more marked in L2/3 (blue; 20-25%) compared to L4 (green; 8-10%) as well as when considering the connections from L4 to L2/3 (red; 12-15%). This tendency inverts at orientation-preference differences of ∼35-50 degrees, consistent with a trend for neurons with near perpendicular orientation preferences to be less likely to have functional connections with each other. Only neurons that were orientation selective by the same criterion used in[37] were considered in this analysis (see methods). Therefore, in accordance with expectations, we confirmed that neuronal pairs with similar orientation preference are indeed more strongly functionally connected and found this trend to be more prominent in L2/3. Interestingly, the reverse trend was observed when considering anticorrelated pairs (z-score<-2.5; suppl. Fig. 3.1), i.e. neurons that have near perpendicular orientation preference are more likely to be negatively functionally connected. A similar analysis was performed by comparing receptive field shape similarity (see methods) and plotting the fraction of significant pairwise connections and their strength as a function of a receptive field similarity index we derived (Figs. 3D, 3C; see Methods). Consistent with the orientation preference analysis, high receptive field shape similarity conferred a higher probability of functional connection. Having said that, it is important to note that functional connections computed during spontaneous activity conditions tend to be more promiscuous than expected, and do not appear to be restricted to neurons with similar receptive field shape or orientation tuning. In sum, although tuning function similarity implies a bias towards stronger functional connectivity, it leaves enough room for neurons with disparate functional properties to also be strongly functionally connected.

First-order Functional Connectivity (1FC) Neighborhoods

To go beyond pairwise correlations, we need to try to parse the structure of functionally connected pairs of neurons into groups. A natural graph to investigate consists of a neuron with its immediate (i.e., first-order) functionally connected neighbors. We call this the "first-order functional connectivity" (1FC) group of the index neuron, and it may be thought of as a simple multi-neuronal communication unit beyond the cell itself. The degree of connectivity of a neuron is the number of its first-order connected neighbors. Neurons with large degrees of connectivity are called "hubs"[38,39] as they represent circuit nodes with a potential for high-volume communication. Figure 4A histograms the degree of connectivity of the neurons in L4 (green) versus layers 2 and 3 plotted together (blue), expressed as a fraction of all neurons in the corresponding layer (excluding the index neuron). Note that the "hub" structure differs across layers. In L2/3, the fraction of neurons with a given degree of connectivity falls approximately exponentially as the degree of the connectivity rises (suppl. Fig. 4.1A), whereas in L4, it remains approximately flat until much higher values. This uniformity suggests L4 networks have less of a hierarchical structure, achieving a more even distribution of the computational load across the nodes, shorter path lengths, and better fault tolerance and robustness. In contrast, L2 networks exhibit a more hierarchical structure, promoting efficient computations and network scalability. Furthermore, balanced connectivity may allow the L4 network, which is the chief recipient of input from the lateral genicular nucleus, to learn to process more effectively a wider-range of input patterns, before passing on the information to L2/3. The difference in the distribution of degrees of connectivity between L4 and L2/3 networks persists for the core network of stronger connections computed over smaller (15-minute long) time intervals. Specifically, the degree of connectivity distribution in L4 exhibits a longer tail (suppl. Fig. 4.5).

To probe whether 1FC groups are indeed groups of neurons "cooperating" with each other, we need to demonstrate that member neurons fire together with higher probability than would be anticipated simply by virtue of being functionally connected to their "parent" neuron. Figure 4B histograms the clustering coefficients of 1FCs

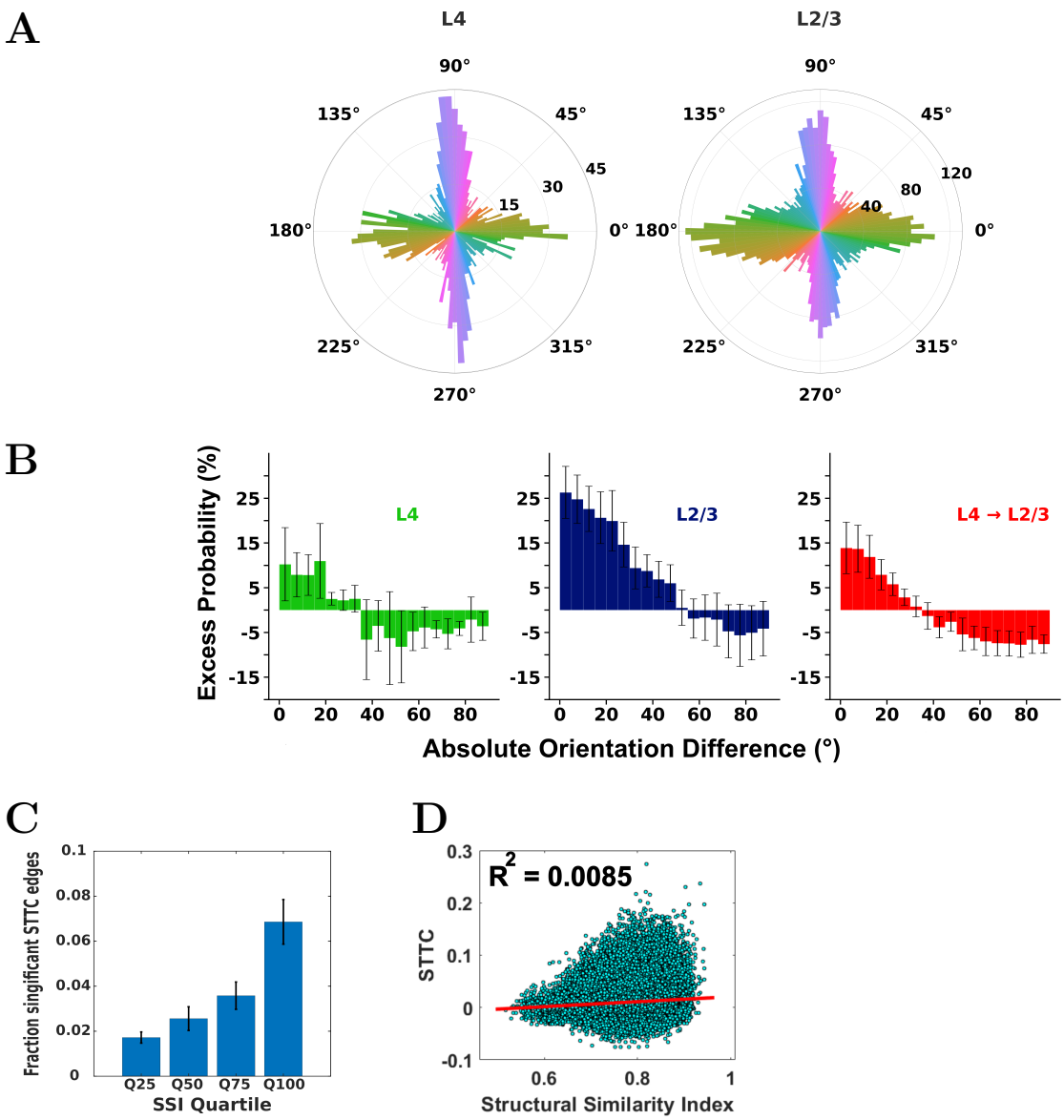

Fig. 3: **Relation of Spontaneous Functional Connectivity to Tuning Properties.** Tuning function similarity implies a bias towards stronger functional connectivity but leaves enough room for neurons with disparate functional properties to also be strongly functionally connected. A) The neurons' direction tuning was estimated as in Fahey P. *et al.*[37]. The bins were colored according to the preferred orientation, with a radial dimension equal to the number of neurons in each bin. This histogram is across all mice. Note that the cardinal bias known to exist among orientation preferences of neurons in mouse V1, which results in a slight rotation concerning the vertical as the eyes were not perfectly aligned with the vertical-horizontal meridians of the monitor, has been corrected here. B) Histogram of the orientation preference difference among neuronal pairs with statistically significant functional correlations (z-score > 4; L4: green, L2/3: blue, L4→L2/3: red) minus that of the null, formed by pairs with not statistically significant functional connections, with z-score from -2 to 2. The difference computed in each bin is normalized by the probability of the null distribution in that bin. The orientation difference between neuronal pairs was estimated as the minimum absolute difference of their strongest amplitude angles computed in the circular [0,180) space (zero identified to 180 degrees); thus, the orientation-difference range is [0, 90] degrees (for more information, see Methods); Error bars: SEM across the five mice examined. C) To explore the trend in more detail, we grouped the cell pairs into quartiles according to the values of the structural similarity between their receptive fields and calculated the fraction of pairs in each

Fig. 3: quartile having an STTC z-score ≥ 4. Bars represent mean fraction of significant STTC pairs in each quartile, error bars = sem, n = 5 mice. A clear difference exists between lowest and highest quartiles in terms of the fraction of functionally connected pairs (Y-axis: proportion between functionally connected (Z $\geq$4) and non-connected pairs (Z<4)) (p = 0.0079, Wilcoxon ranksum test across mice; lowest quartile: 0.017±0.0025, highest quartile: 0.069±0.01). D) Receptive field similarity versus strength of functional connectivity: high similarity in receptive field maps does not imply stronger functional connectivity between cells on average across population. Relationship between STTC correlation coefficient and structural similarity of receptive field maps in visually responsive cells of an example mouse. Although there is a trend of cells with strongly similar receptive field maps also having a higher probability of stronger STTC connection, this trend is weak and non-linear ($R^2 = 0.0085$, red line shows linear fit).

---

groups of L4 (green) versus L2/3 (blue) neurons, after excluding imaging frames that contain firing events of the neuron itself. The clustering coefficient of the 1FC group of a neuron is the ratio of the number of significant pairwise functional connections between its 1FC group members divided by the number of all possible pairwise connections between them. Gray histograms illustrate the clustering coefficients of a null distribution generated by groups of the same size and layer, formed by selecting neurons randomly. Clustering coefficients of 1FC groups tend to be distributed at much higher values than the corresponding null distributions (mean ± standard deviation in L4: ∼0.55 ± 0.04 versus ∼0.22 ± 0.06 for the null, while in L2/3 ∼0.45 ± 0.04 vs. ∼0.12 ± 0.03, respectively), reinforcing the idea that 1FC groups act as "*cooperative*" multi-neuronal units that may serve as computational modules.

We examined the architecture of the network of statistically significant functional connections (i.e., STTC z-score > 4) within each layer and try to understand its implications for how information is processed by the layer. In concordance with the higher degree of connectivity we observed in L4 (Fig. 4A), L4-1FC groups are significantly more densely interconnected (have higher clustering coefficients) compared to 1FC groups in L2/3 (Fig. 4H; Welch's t-test p-value=0.006). Overall, the functional connectivity networks in both L4 and L2/3 exhibit strong small-world characteristics, as reflected by their short average path lengths and relatively large clustering coefficients, when compared with the corresponding random Erdős–Rényi random network graphs and regular "ring" networks (suppl. Fig. 4.8; see methods for the generation of the corresponding theoretical graphs)[38]. Small world networks are advantageous in their ability to balance efficiency of information transfer with local specialization, making them highly effective and resilient across a wide range of complex system computations. To assess network robustness, we examined whether or not the network consists of a giant (connected) component. By definition, a giant component (of a network) includes the majority of nodes of the network and any two of its nodes are connected via some path. We also employed the Molloy-Reed index, the ratio of the mean squared degree of connectivity over the mean degree of connectivity (see Methods). A random network with Molloy-Reed index above 2 indicates robustness, in the sense that a large fraction of the nodes in the network are interconnected, enhancing the network's resilience. Suppl. Fig. 4.9 demonstrates that V1 L2, L3 and L4 networks are all highly robust and remain well interconnected across a large range of z-score thresholds used to define functional connectivity (supplementary Section 4.2, suppl. Fig. 4.9). So far, we have been discussing functional connectivity within individual cortical laminae. In order to try to understand how patterns of activity are communicated between layers, we next examine inter-layer functional connectivity groups, i.e. 1FC groups that individual L2/3 neurons form with neurons in L4. Such groups may be loosely viewed as the group of L4 cells that provide putative input to the L2/3 neuron.

Interestingly, even for very high z-score thresholds, the resulting functional networks at both layers remain well-connected.

Inter−layer Functional Connectivity: Putative L4 Input Groups to L2/3 Pyramidal Neurons

Figures 4C-H illustrate L4 to L2/3 inter-layer pairwise functional connectivity characteristics. The percentage of significant inter-layer functional connectivity links from L4 to L2/3 (red) is similar to that observed within L2/3 (blue), a little lower than the one observed in L4 (green) (Fig. 4E). The distribution of significant STTC

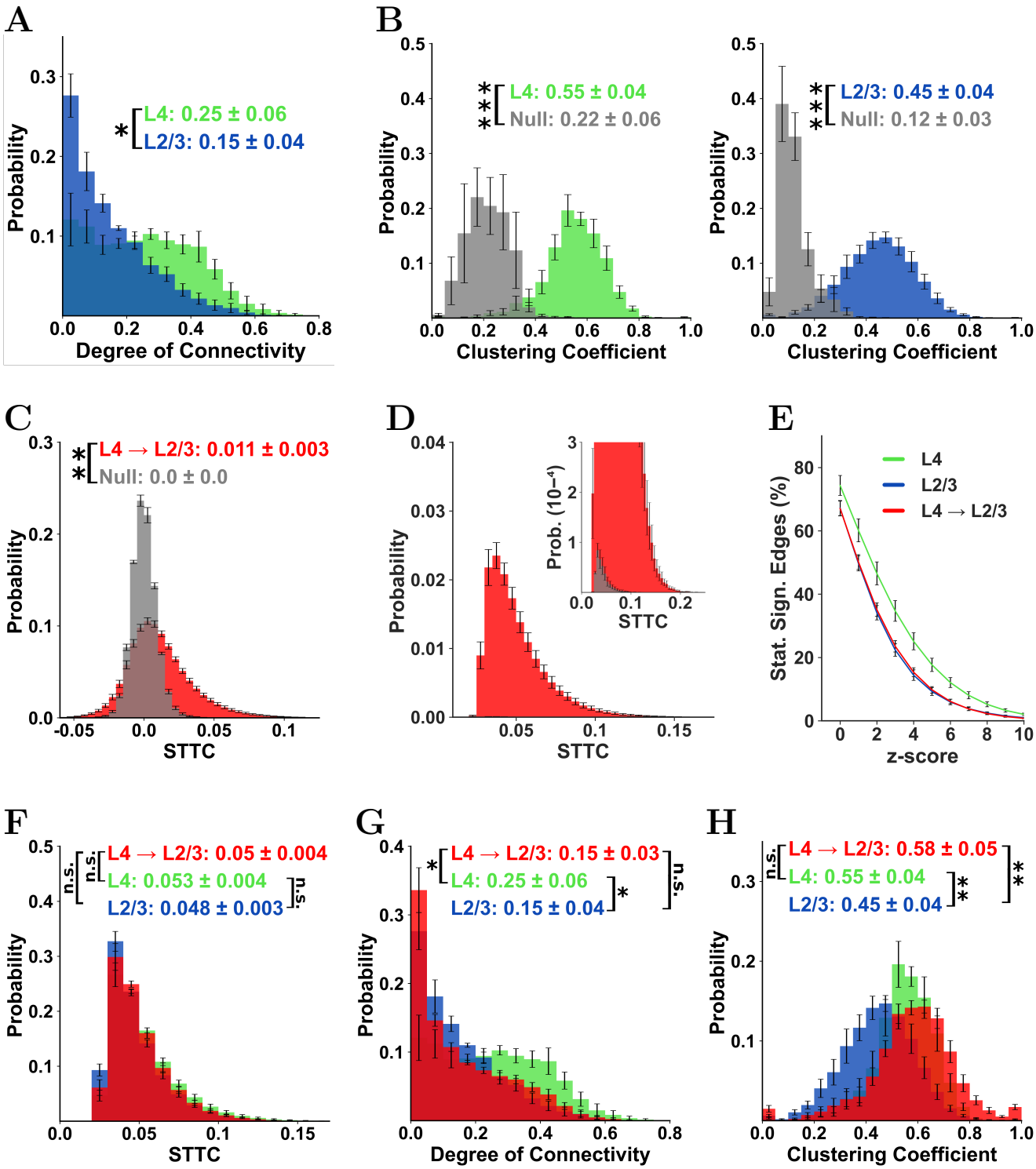

Fig. 4: First-order Functional Connected (1FC) Groups. We define 1FC to be the first-order functionally connected neighbors of a neuron. A) Histograms of the degree of connectivity of neurons in layer 4 (green) and layer 2/3 (blue), expressed as a fraction of the total number of neurons belonging to layer 4 and layer 2/3 FOV, respectively. Only edges with statistically significant positive STTC (z-score > 4) were included in the calculation. The two distributions are clearly different. B) Histogram of clustering coefficients of 1FC groups of L4 (green) and L2/3 (blue) neurons, computed *after excluding* the frames containing calcium events of the neurons themselves. The gray histogram represents a null distribution constructed by selecting at random commensurate groups that

Fig. 4: are not functionally connected to the reference neuron. Error bars: SEM across the 5 mice examined. For each layer case, the sample mean of the degree of connectivity and clustering coefficient of each neuronal population across the five mice along with their standard deviation are reported. C) The distribution of actual (red) and null (computed after random circular shifting; gray) STTC weights from L4 to L2/3. D) Histogram containing only statistically significant (z-score >4) positive functional connections. The magnified inset reveals the tail of the null distribution. E) Percentage of statistically significant connections as a function of significance threshold (z-score) for L4 (green), L2/3 (blue), and L4→ L2/3 (red). The latter two curves are nearly identical. F) Histogram of STTC weights of statistically significant (z-score >4) positive functional correlations. The distributions are remarkably similar both within and across layers. G) The histogram of normalized degrees of connectivity from L4 → L2/3 (red) is similar to that within L2/3 (blue), contrasting with the uniform distribution seen in L4 (green), which reaches higher degree of connectivity values. H) Distribution of clustering coefficients of L2/3 neuron 1FC groups in L4 (across laminae; red) is shifted to the right compared to clustering coefficient distributions within L2/3 (blue) or L4 (green). Note that for the estimation of the clustering coefficient, the imaging frames in which the "index" L2/3 neuron fires have been excluded to eliminate bias. Figure insets represent the mean ± standard deviation of the sample means across mice (n=5); Error bars: standard error of the mean (SEM) across mice (n=5). P-values: "*": < 0.05; "**": < 0.01; "***": < 0.001, and "n.s.": non statistically significant. The highest p-value obtained from the permutation of means, the Welch's t-test, and the ANOVA F-test is reported.

---

weight values is essentially identical to that computed within different cortical layers (Fig. 4F), suggesting that the distribution of pairwise functional correlation strengths is relatively conserved across cortical circuitry. The first-order inter-layer functional connectivity (1FC) groups of L2/3 neurons in L4 have similar degrees of connectivity but higher clustering coefficients compared to intra-layer L2/3 1FC groups (Fig. 4G-H) suggesting that their members are more in synchrony with each other.

The 1FC group of a L2/3 neuron in L4 can be thought of as constituting the putative input group for this neuron. It is therefore natural to ask to what degree synchronous activity (i.e. cofiring events) within these putative L4 input groups can predict the activity of the corresponding L2/3 neurons.

L4-1FC group cofiring predicts the probability of calcium events in L2/3 neurons

We plot the probability that a L2/3 neuron fires a calcium event per imaging frame (155ms) as a function of the total number of "cofiring events" that occur across its putative input group in the same frame. Fig. 5A illustrates two-example L2/3 neurons, whose probability of firing increases with the number of cofiring events in their respective L4-1FC groups, nearly approaching 1 at high cofiring values. In contrast, the gray line (control), which represents the prediction arising using the same number of randomly selected L4 neurons that *do not* have a significant functional connection with the L2/3 unit, remains flat. The majority of neurons exhibit a monotonic increase in their probability of firing that is well-fit by a ReLU function (see methods). Fig. 5B histograms the normalized root mean square error (RMSE) values for ReLU (red) vs. linear (black) fits, indicating the superiority of the former (lower RMSE values).

Fig. 5C histograms the corresponding goodness of fit R^2 values obtained by standard error of the mean weighted linear regression, merging high-cofiring bins that contain less than 10 instances of cofiring (see methods). Note that the quality of the fits is very good for most neurons. Fig. 5D histograms the slope of the linear part of the ReLU fits for neurons with $R^2 \geq 0.8$, yielding a measure of how much the probability of firing of L2/3 neurons increases per ten added cofiring events in their 1FC group. The null (gray) distribution is centered approximately at zero as expected. We used the ReLU fits to extrapolate how many cofiring events are needed to yield a probability of firing equal to 1, i.e. to predict with certainty that the L2/3 neuron will fire. Fig. 5E histograms these values for ReLU fits with $R^2 \geq 0.8$. Across L2/3 neurons, the mean number of cofiring events needed to strongly drive pyramidal neurons is $\sim$70, roughly commensurate to prior estimates made in a different context by Shadlen and Newsome[40]. As many as $\sim$51% of L2/3 neurons with $R^2 \geq 0.8$, would be driven with near certainty, if 25-75 cofiring events occur in their L4-1FC group. For comparison, Fig. 5F plots the *actual* (not extrapolated) *maximum probability prediction* in our data.

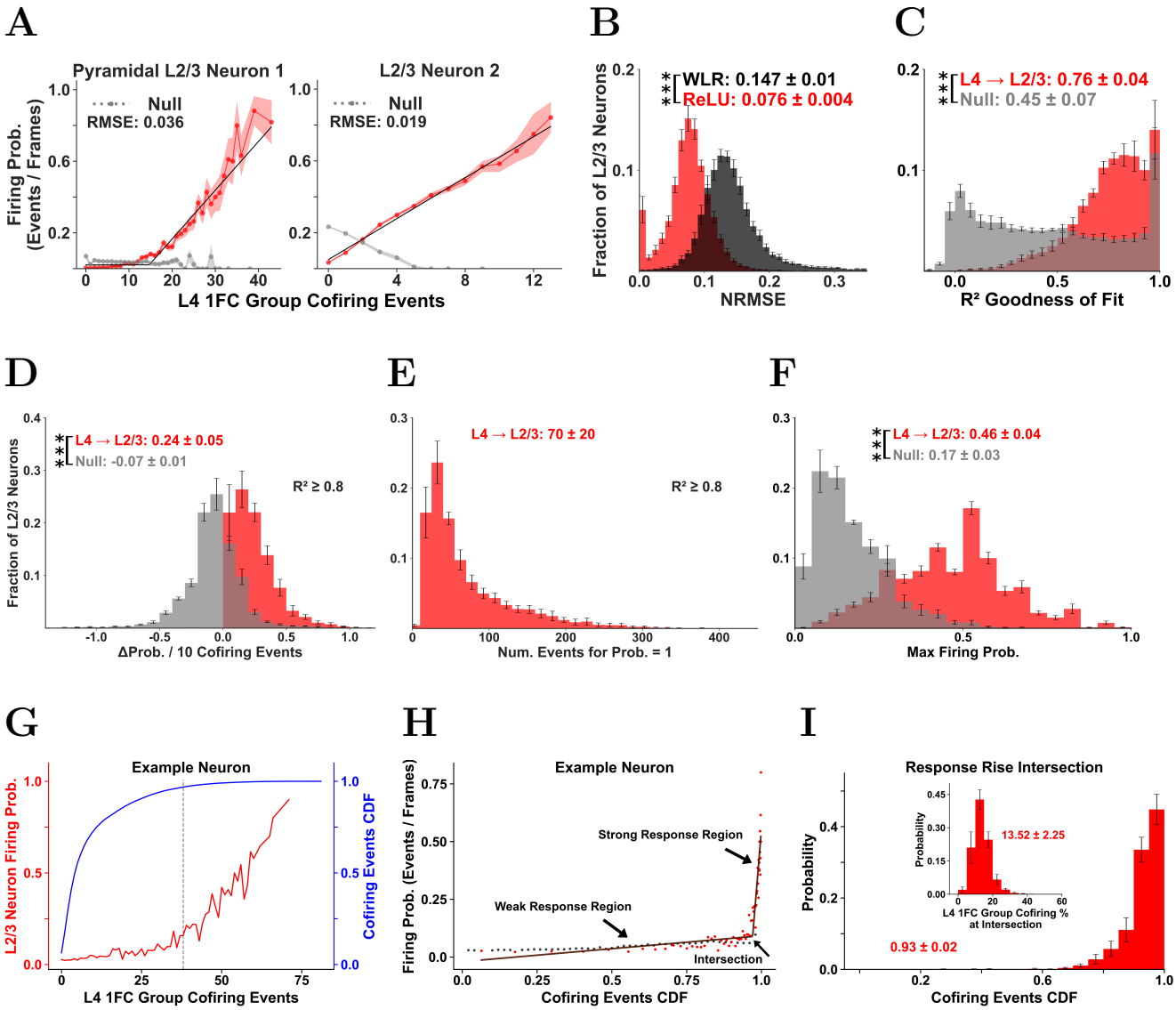

Fig. 5: **Predicting L2/3 pyramidal neuron activity from the cofiring of their L4 1FC groups**. A) Calcium event firing probability of two example L2/3 pyramidal neurons as a function of the number of cofiring events in their L4 1FC (putative input) groups (red line). Shaded region: SEM across cofiring events. Black Line: Left: ReLU fit, Right: Linear fit. Gray dashed line: Null (control; see methods). In contrast to the observed, the response of the null remains approximately flat, and has fewer cofiring events of higher order. B) Comparison of the normalized root mean square error (RMSE) between the linear (black) and the ReLU fits (red), indicating the superiority of the latter. C) Histogram of R^2 values resulting from the ReLU fits, appropriately weighted by the standard error of each point (see methods). Note that the majority of the fits are acceptable (>0.75) in contrast to the null responses (gray), which exhibit significantly worse fits. D) Histogram of the slope of the fit, measured as the increase in the probability of firing per 10 additional cofiring events (per frame), derived from fits with R^2 ≥0.8; E) Extrapolated number of cofiring events that yield a probability of firing = 1, derived from fits with R^2 ≥0.8; F) Maximum firing probability of the actual response function versus the null; G) The cofiring CDF of the layer 4 1FC group (blue line) plotted together with the response function (red line) for an example L2/3 pyramidal neuron. Dashed line: number of cofiring events that correspond to the approximate intersection of the no-response and response regions. It is clear that this L2/3 neuron fires for large and relatively rare, cofiring events. H) Scatterplot of the data of the same neuron presented in **5G**, as a function of the CDF probability of cofiring events. This neuron illustrates the typical response we observed across layer 2/3 cells, which exhibits two regions: i) a weak nearly flat response region and ii) an abrupt and steeply rising one, which emerges near the right tail

Fig. 5: of the cofiring event distribution, when cofiring events are large and relatively low probability. The response can be fitted by two separate linear trends, shown here. The first line has a slope close to 0 and represents the weak response regime, while the second demonstrates the sharply rising neuronal response. For this neuron, the intersection of these two regions occurs approximately at CDF=0.96. That is, only 4% of frames (rare events) have a sufficiently large number of L4-1FC cofiring events to make the corresponding L2/3 neuron fire. Grey dots correspond to null distribution as in **Fig. 5A.** I) Histogram of the CDF value of cofiring events corresponding to the start of the sharply rising response's intersection (of the two lines that fit the response). Inset: Histogram of L4-1FC group cofiring percentages that correspond to the CDF value at the response intersection. On average, the switch to the fast-rising response regime for L2/3 neurons occurs at CDF=0.93 for L2/3 neurons, which corresponds to approximately 13% of its putative input group firing together. Only the L2/3 neurons reaching firing probability ≥ 0.6 and have a ReLU fitting $R^2 \geq 0.8$ have been used for Figs. 5G-I. L2/3 neurons whose response region (fig. H) had a slope < 1 were excluded ($\sim$13% of neurons on average across mice). The slope is estimated as the ratio of the difference of the likelihood of response at two distinct numbers of cofiring events over the difference of their corresponding ECDFs. Histogram mean $\pm$ standard deviation across mice (n=5) are given as insets in Figs. **B-F, I**; Error bars: SEM across the five mice examined. P-values: "*" < 0.05, "**"< 0.01, "***" < 0.001. The highest p-value obtained from the permutation of means, the Welch's t-test, and the ANOVA F-test is reported.

The two regimes of the response of L2/3 neurons

We demonstrated that the response of L2/3 neurons depends on the number of cofiring events that occur within their L4-1FC (putative input) groups. We further explored the relationship between the slope of the prediction function and the distribution of cofiring events within the L4-1FC groups. Interpolating the slope of the prediction function, we found that L2/3 neurons tend to remain silent for the majority ($\sim$93%) of cofiring events occurring within their L4-1FC groups, the probability of firing beginning to *sharply rise* approximately when cofiring event size crosses into the largest decile (Fig. 5H). Fig. 5H shows the response function of an example L2/3 neuron versus the number of cofiring events in its L4 putative input group (red dots). It is clear the neuron's firing has two regimes approximately fitted by two lines. The first line has a slope close to 0 and represents the regime of *no or weak response*, while the second has a positive slope and represents the *significant response regime*. For this neuron, the intersection of the two regions occurs at approximately CDF=0.96. Thus, only 4% of frames have a sufficiently large number of cofiring events to induce the L2/3 neuron to fire (relatively rare events, see also Fig. 5G). Contrast this with the null distribution (grey dots, Fig. 5H), computed from an equal number of L4 neurons that do not belong to the L2/3 neuron's putative input group, which remains flat throughout. On average, the switch from the weak response to the strong response regime for L2/3 neurons occurs at CDF=0.93 (i.e. for 7% of the highest cofiring events in their putative input groups; Fig. 5I). This value corresponds to $\geq$ 13% of the putative input group neurons firing together (cofiring percentage; Fig. 5I, inset). Figs. 5I, 5G include all L2/3 neurons that reached a maximum firing probability of 0.6 or more and have a good ReLU fitting ($R^2 \geq 0.8$); qualitatively, similar results are obtained under other thresholds. In sum, L2/3 neurons respond stochastically, but their reliability of firing rises sharply only when a high number of cofiring events occurs in their putative input group. The point at which this transition occurs is set to ensure firing remains sparse across the population of L2/3 neurons.

Influence of different neuronal subnetworks on L2/3 neuron activity prediction

L2/3 neuronal activity can be predicted to a significant degree as a function of the cofiring of their functionally connected L4 putative input group. However, the transmission of information from L4 neurons to an L2/3 neuron does not happen in isolation. Active together cortical subnetworks influence this prediction. Fully resolving the dependence of L2/3 neuron firing on these diverse interdependent, inhibitory, or excitatory influences is beyond the scope of the current manuscript. However, we will comment on the effect of cofiring activity **i)** in the neighborhood of positively correlated neurons within L2/3, and **ii)** in the neighborhood of anti-correlated neurons within L4.

By itself, cofiring activity in a L2/3-neuron's intra-layer 1FC group (L2/3 1FC) predicts its probability of firing significantly above null expectations (blue line; Fig. 6A), though not as well as cofiring activity in its L4-1FC (putative input group; red line in Fig. 6A). In fact, cofiring in these two neuronal ensembles can act synergistically. Figure 6B demonstrates that the firing probability of L2/3 neurons for a given level of cofiring in their L4-1FC group is significantly enhanced when their L2/3 1FC group fires concomitantly. The black line illustrates the mean probability of firing across L2/3 neurons as a function of cofiring in their L4-1FC groups averaged across all mice

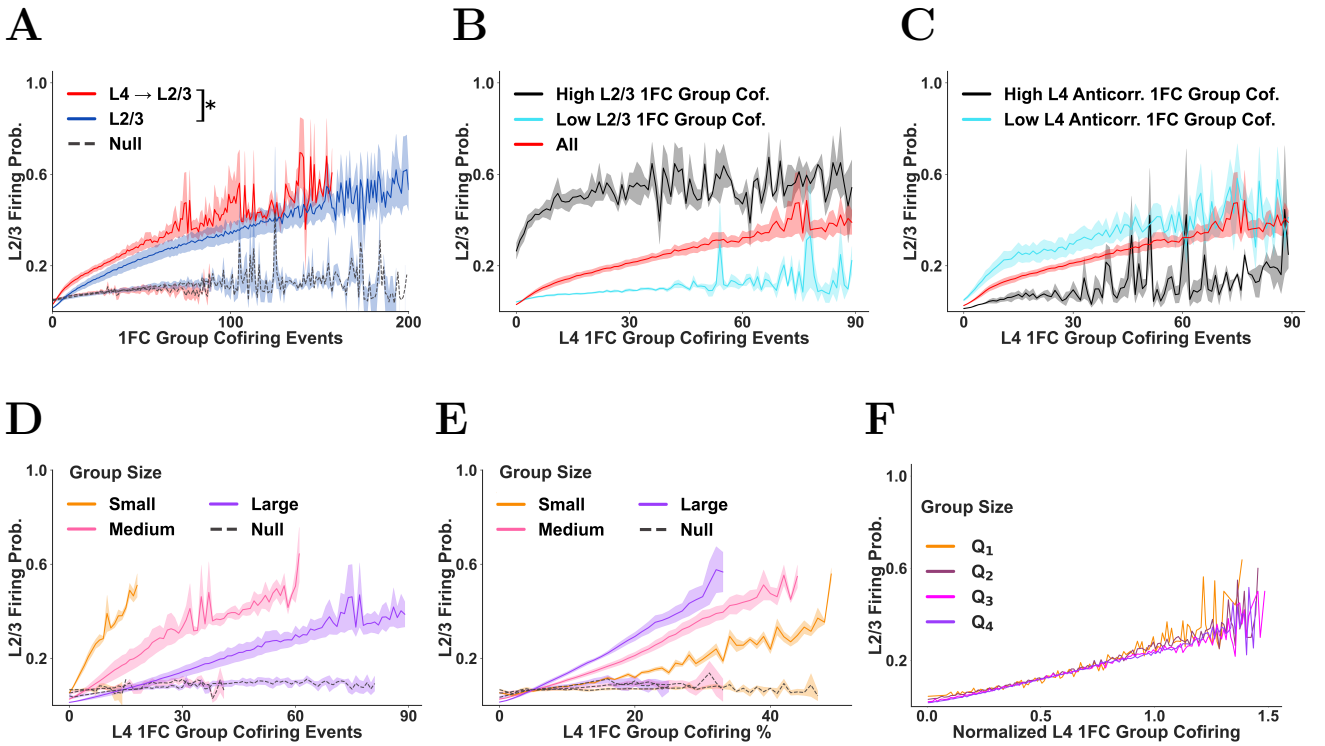

Fig. 6: **Influence of different neuronal subnetworks on L2/3 neuron activity prediction.** A) Red line: Average probability of firing of L2/3 neurons as a function of the number of co-firing events in their L4 1FC groups, at the same imaging frame. Blue line: As in (A) but based on cofiring events in the L2/3-1FC group. Dashed Lines: Prediction based on randomly selected L4 neuronal groups of the same size that do not overlap with the L2/3 neuron's 1FC L4 group. B) Red Line: As in (A), prediction of the probability of firing of L2/3 neurons from their L4 putative input groups. Black Line: As in (A) but now considering only frames in which there is also substantial (>40%) cofiring activity within the neuron's L2/3 1FC group. Cyan: Like Black but now considering only frames in which there is low (5-10%) cofiring activity within the neuron's L2/3 1FC group. C) Red Line: As in (A). Black Line: As in (A) but now considering only frames in which there is also substantial (20-80%) cofiring activity within the neuron's anti-correlated L4 1FC group. Cyan: Like black but now considering only frames in which there is low (<5%) cofiring activity within the neuron's anti-correlated L4 1FC group. L2/3 neurons with L4 correlated or anticorrelated groups with 10 neurons or less have been excluded from the analysis. D) Average probability of firing of L2/3 neurons as a function of the number of co-firing events in their L4 1FC groups. Yellow: L2/3 neurons with L4 1FC *group sizes* belonging to the smallest quartile (Q0-Q25). Purple: L4 1FC group sizes belonging to the largest quartile (Q75-Q100). Pink: L4 1FC group sizes belonging to the middle quartile (Q37.5-Q62.5). Note that fewer cofiring events translate into a larger probability of firing for small groups (orange) compared to medium or large ones. E) As in (D), except the x-axis is expressed as the percentage of neurons of the L4 1FC group that cofire. The order in the size of the slopes is reversed: now a smaller percentage of cofiring neurons translates in larger probability of firing for large groups (purple) compared to medium or small ones. F) Interestingly, there is a power of N (size of the L4 1FC group), normalizing by which results in identical slope for all groups of different sizes (quartiles Q1 to Q4). The normalization is done by dividing by the L4 1FC group size raised to the power of the constant. Here the plot shows one example mouse with a normalization constant of a ∼0.7. Across mice the constant varied from ∼0.6-0.7 (see Methods for a detailed discussion). Groups with sizes less than 5 have been discarded from Q1 to minimize low number bias. Shaded regions: SEM across mice (n=5).

---

under the condition that L2/3 1FC groups exhibit >40% cofiring. It lies markedly above the red curve, which places no condition on L2/3 1FC firing, indicating clear facilitation. Conversely, when 1FC L2/3 cofiring is low, the probability of L2/3 firing (cyan line) dips near the null position, well below the red line. These observations

demonstrate that the level of cofiring within the L2/3 1FC group is capable of modulating the probability of firing of L2/3 neurons, even when the level of cofiring in their L4-1FC group is held fixed. It is therefore in principle possible that top-down influences may use this strategy to modulate the information transmission from L4 to L2/3.

Figure 6C demonstrates the effect of cofiring activity within the L2/3 neuron's *anti-correlated* group in L4. As expected, when activity is high within the anti-correlated L4-1FC group, the probability of firing decreases (black line), while conversely when activity is low the probability of firing increases (cyan line). These statistical relationships are starting to reveal how activity in distinct population ensembles influences the firing of cortical neurons, at least under spontaneous activity conditions. Although we cannot generally infer causality directly from these statistical relationships, they likely contain important clues about how dynamic patterns of activity emerge and propagate within cortical networks under spontaneous conditions.

L4 functional connectivity group size impacts prediction of L2/3 neuron responses

The previous section demonstrated that L2/3 neuron firing probability can be estimated as a function of the level of cofiring within their L4 putative input groups. The slope of this response function depends on putative input group size. Fig. 6D plots the average firing probability of L2/3 neurons as a function of the number of cofiring events separately for three different putative input group (L4-1FC group) size quartiles: small (Q0-Q25; orange), middle (Q37.5-Q62.5; pink) and large (Q75-Q100; purple). Evidently, the smaller the L4-1FC group size, the steeper the slope of the response function, indicating a sharper rise in the probability of firing per cofiring event for L2/3 neurons with small L4-1FC groups.

A natural question is whether the observed difference in slope can be explained by a *process of normalization*. For example, it is possible that the L2/3 neuron output gets adjusted depending on the dynamic range of inputs it receives, which depends on the number (N) of its putative L4-input neurons. The adjustment may take the form of divisive normalization[41]. We, therefore, tested whether expressing cofiring events as the percentage of neurons cofiring in the L4-1FC group can eliminate the observed slope differences. Fig. 6E shows that this form of normalization fails; in fact, it overcorrects: the slope order reverses and smaller groups have now lower slopes, i.e. requiring a bigger percentage of their L4 putative input neurons to fire to achieve the same probability of firing as L2/3 neurons with larger L4 functional connectivity groups. Normalizing by the mean aggregate activity within the L4-1FC group also fails similarly. Interestingly, there is a normalization that works for bringing the slopes together (Fig. 6F) and this is dividing by N^a, where a is an exponent ranging from ∼0.6-0.7 for each of the 5 mice tested. The fact that this exponent is approximately preserved across mice and across different group sizes suggests that it may reflect a network property. A simple model that gives some intuition about the potential reason behind such a normalization is discussed in supplementary material. In brief, under the approximate assumption that L4 neurons fire independently with the same probability, normalizing their L4 putative input group by $N^{0.5}$ has the effect of forcing L2/3 neurons to respond as linear functions of the same probability distribution, independent of the size (N) of their L4-1FC group. Although $a = 0.5$ is clearly less than the $0.6-0.7$ we found experimentally, it is possible that this difference might be attributed to the existence of correlations or to differences in the probability of firing among different L4 neurons.

One may wonder whether the different response functions of L2/3 neurons with small L4-1FC groups simply reflect the possibility that we failed to image other, presumably out-of-plane, neurons with which they are functionally connected. To test this hypothesis, we examined how L2/3 neurons with large L4-1FC groups behave as a function of cofiring, when the latter is restricted to small subsets of their large L4-1FC groups, commensurate to the small L4-1FC groups. We found that the behavior of L2/3 neurons with small L4-1FC groups was distinct from that of these *control subsets* (Suppl. Figs. 7.9, 5.6). This was particularly evident during epochs when the aggregate population activity is not significantly high (Suppl. Fig. 7.6). Therefore, we conclude that L2/3 neurons with small L4-1FC groups have distinct properties that do not represent artifacts of imaging bias.

The above observations argue that the number of cofiring events in a L2/3 neuron's L4-1FC group is important for relaying activity from L4 to L2/3. This claim is also consistent with the observation that the accuracy of predicting L2/3 neuron activity does not improve when, in addition to the *number of cofiring events* of its L4-1FC group, we include the entire vector that indicates the identity of each L4-1FC group member and whether or not it fires at a certain frame. This has been tested using an SVM classifier with linear kernel, random forest, Naive Bayesian, and logistic regression (see Suppl. Figure 5.4).

Our analysis has been performed in the absence of stimulus under spontaneous conditions. However, internal factors can still potentially modulate the functional connectivity properties we describe. Naturally, functional connectivity is not an immutable property but exhibits a highly dynamic dance of changing allegiances (functional

connections). In the next section, we explore the dynamic nature of pairwise functional connections, the groups that we have defined, and how they are modulated by parameters that reflect brain states.

Modulation of Functional Connectivity by Variables Associated with Internal States

Both dynamic changes in the aggregate neural population activity and changes in the pupillary diameter over time have been associated with the general state of alertness and attentional effort exerted by the animal[42,43]. We, therefore, asked how functional connectivity is modulated by pupillary-size and aggregate population activity dynamics, which act as proxy measures reflecting the animal's internal state.

A. Dependence on aggregate population activity

We computed the event triggered average (ETA) of the normalized aggregate neural activity observed in L4, relative to the firing of individual L2/3 neurons (Fig. 7A; see methods). Interestingly, L2/3 neurons with large L4-1FC groups tend to fire when L4 population activity is high, whereas L2/3 neurons with small L4-1FC groups show little, if any, dependence on aggregate firing rate (Figs. 7A,7B). Notably, the trend persists after removing the L4-1FC group of the index L2/3 neuron from the L4 population, so it is not a trivial consequence of the L4-1FC group size. This suggests that L2/3 neurons with smaller L4-1FC groups couple increasingly weakly to the overall neural population activity. In fact, L2/3 neurons with large L4-1FC groups tend to fire approximately at the peak of relatively strong aggregate population activity modulations (positive aggregate activity deviations from the man corresponding on average to a z-score of 0.5-0.8; purple curves in Fig. 7B). In contrast, the smallest L4-1FC groups tend to fire during epochs of population activity that are slightly suppressed relative to the mean (yellow curves in Fig. 7B), though they still tend to fire near a local peak in aggregate activity.

Prior work has categorized neurons into those whose firing correlates with overall activity ("choristers") and those independent of it ("soloists")[44]. Our findings align with this: L2/3 neurons with larger L4 groups (similar to "choristers") are more influenced by overall activity, while those with smaller groups ("soloists") show minimal modulation (Figs. 7A,B). This is further supported by the observation that L2/3 neurons with small L4-1FC groups maintain a consistent firing rate across different aggregate population activity levels, unlike those with large L4-1FC groups, which exhibit increased activity during high aggregate activity periods (Fig. 7D).

The proportion of significant functional connections and clustering coefficients in 1FC groups within and across layers rises during periods of high aggregate neural activity (Suppl. Figs. 7.4A,B, respectively). In contrast, the distribution of functional connectivity weights remains relatively invariant across different aggregate activity levels (Suppl. Fig. 7.5B), reflecting a potential universal property of the cortical circuitry for maintaining stability and avoiding runaway excitation. Having said that, the tail of the distribution towards higher functional connectivity strengths can vary with behavioral state (e.g., suppl. Figs. 7.4B, 7.5), likely reflecting a higher level of activity within certain behaviorally relevant subnetworks. Notably, while the overall distribution of these connections remains stable, the frequency of higher values varies with behavioral states, possibly due to certain subnetworks being more active under specific behavioral states.

B. Dependence on Pupillary Dynamics

L2/3 neurons exhibit different modulation patterns with respect to pupillary dynamics. Figure 7F illustrates calcium event-triggered averages (ETAs) of L2/3 neurons with respect to the normalized pupil radius. Neurons with large L4-1FC groups (neurons 1,2) fire near the pupil size nadir (negative peak of the ETA), whereas neurons with small L4-1FC groups tend to be much less sensitive to pupilary size modulations and tend to fire during the decrease or increase of the pupil radius (neurons 3 and 4, respectively). The morphology of the ETA divides L2/3 pyramidal neurons into two mutually exclusive groups and the Pearson correlation of their ETA shapes shows two distinct peaks, one highly correlated ($\sim$+1) and the other highly anticorrelated ($\sim$-1) (Fig. 7H). Again, the behavior of L2/3 neurons with large versus small L4-1FC groups differ also with respect to pupillary dynamics. L2/3 neurons with small L4-1FC groups exhibit two subpopulations with anticorrelated ETAs. Figure 7G illustrates the average ETA of the pupillary size of all L2/3 neurons with small (lowest quartile; orange) groups versus that of L2/3 neurons with large (highest quartile; purple) groups. The ETAs of neurons with small (lowest quartile) groups are essentially flat as these neurons appear to fire in no fixed relationship to pupillary dynamics (Fig. 7G). In contrast, L2/3 neurons with large (highest quartile) groups tend to fire when the pupil is at or near its minimum size. Interestingly, *pairs of L2/3 neurons with small L4-1FC group sizes tend to fire independently* compared to

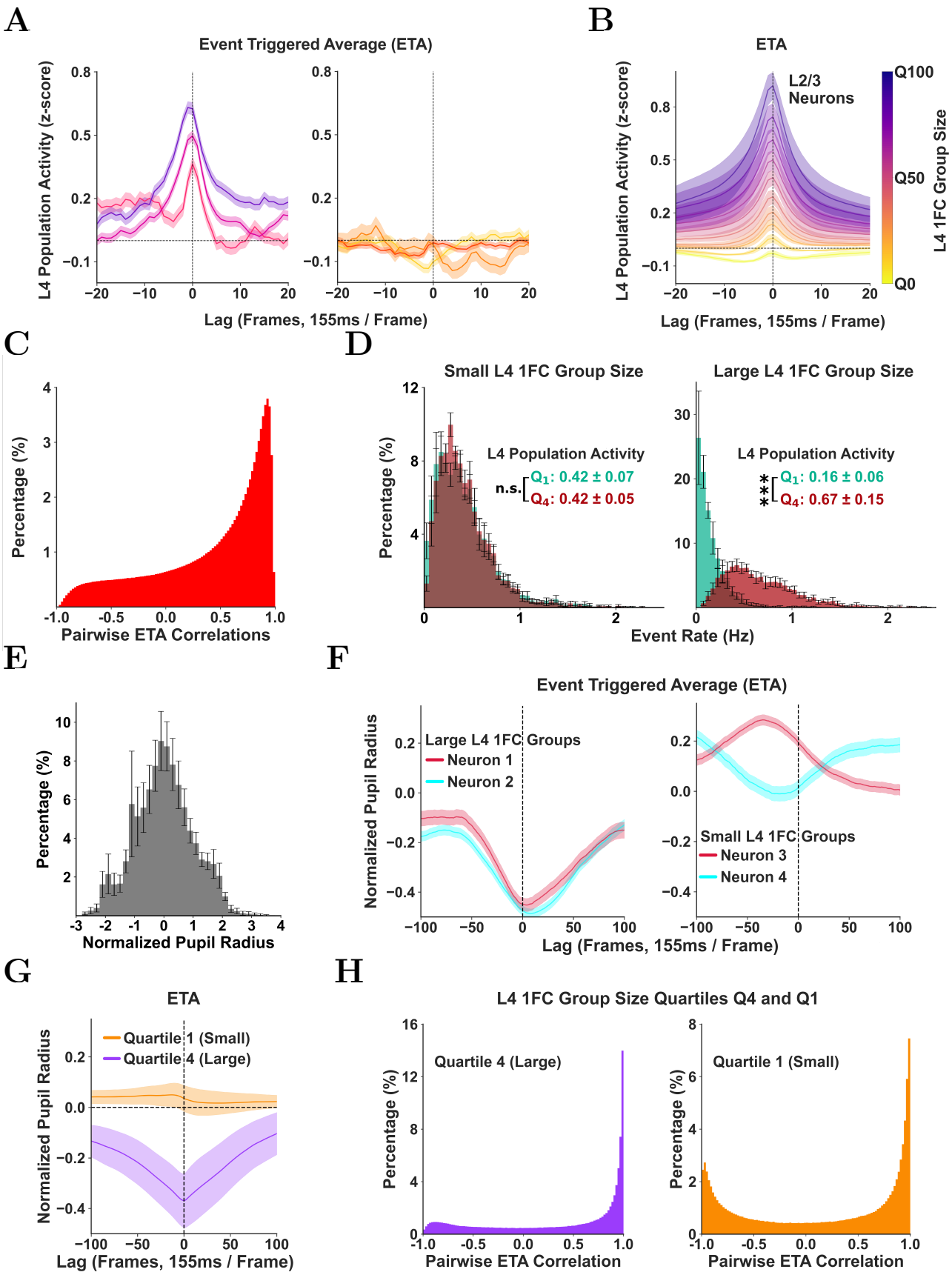

Fig. 7: **Modulation of Functional Connectivity by Population Activity** (Fig. A-D) **and Pupillary Size**

Fig. 7: (Figs. E-H). A) Event triggered average (ETA) of the aggregate L4 neuronal activity for six L2/3 neurons illustrating typical behavior, three with large (left panel) versus three with small (right panel) L4-1FC groups. Time is measured in imaging frames (155 ms) from the time of a calcium event fired by the L2/3 neuron (time zero). L2/3 neurons with large L4-1FC groups tend to fire when L4 population activity is high, whereas L2/3 neurons with small L4-1FC groups show little, if any, dependence on aggregate firing rate. B) ETAs computed as in (A) for L2/3 neurons with different L4-1FC sizes. This confirms that the coupling to aggregate L4 population activity is weaker for neurons with small L4-1FC sizes. The shape of the ETA is also different. For L2/3 neurons with groups of large sizes, L4 population activity increases prior to the firing event, which tends to occur at the peak of the population wave of activity. For L2/3 neurons with small L4 groups, the modulation is much weaker and there appears to be an epoch of aggregate activity suppression before and after the firing event. Overall neuronal behavior exhibits a continuum rather than splitting dichotomously into two discreet categories. C) Histogram of pairwise Pearson correlations between ETA shapes across all pairs of L2/3 neurons. There is a peak at 1 with a long tail towards -1, suggesting that the behavior of most neurons relative to the aggregate population activity is shaped similarly. D) Calcium event rates of L2/3 neurons that have small L4-1FC groups do not change much with aggregate population activity. Left: Histogram of calcium event rates of L2/3 neurons with small (first quartile) L4-1FC group sizes plotted for a high (Q4; brown-grenat) versus a low (Q1; green-turquoise) epoch of aggregate L4 population activity. The event rate of the L2/3 neurons with small L4-1FC groups does not change significantly across the two population firing epochs. Right: Histogram of calcium event rates of L2/3 neurons with large (fourth quartile) L4-1FC group sizes plotted for a high (Q4; brown-grenat) versus a low (Q1; green-turquoise) epoch of aggregate L4 population activity. Bins of 0.05 Hz. In contrast to L2/3 neurons with small L4-1FC groups, the event rate of L2/3 neurons with large L4-1FC groups increases as the aggregate population activity increases. Inset values indicate the mean $\pm$ standard deviation across mice (n=5); Error bars correspond to SEM across mice (n=5). E) Histogram of the normalized pupil radius within each imaging frame, centered at the mean pupil size set at zero and expressed as a z-score per mouse then averaged across mice. F) L2/3 neuron calcium event-triggered average with respect to pupil radius for two example L2/3 neurons with large L4-1FC groups (largest quartile; left) and two L2/3 example neurons with small L4-1FC groups (first quartile; right). G) ETA on pupil radius of L2/3 recipient neurons that have small (quartile 1; yellow line) vs. large (quartile 4; purple) L4-1FC groups, respectively. Note that L2/3 neurons with small L4-1FC groups tend to fire on average with a weak, if any, dependence on pupil size, while L2/3 neurons with large L4-1FC groups tend to fire when pupil size is low. Time is measured in imaging frames (155 ms). H) Left: distribution of pairwise Pearson correlation coefficients across pupil size event-triggered averages of all pairs of L2/3 neurons with large L4-1FC groups. ETA responses appear to be generally highly correlated, with a large peak at 1 and a long but low tail extending to negative correlation values. Right: distribution of pairwise Pearson correlation coefficient across pupil size event triggered averages of all pairs of L2/3 neurons with small L4 1FC groups. Time is measured in imaging frames (155 ms). Pupil size values were recorded at a higher frequency but were then averaged at the imaging frame. ETAs were computed over a range of [-100, 100] frames. Error bars throughout represent the standard error of the mean; P-values: "*" < 0.05; "**" < 0.01; "***" < 0.001, and "n.s.": non statistically significant. The highest p-value obtained from the permutation of means, the Welch's t-test, and the ANOVA F-test is reported.

---

pairs of L2/3 neurons with large L4-1FC groups (Suppl. Fig. 5.3), and are therefore akin to the "soloists" proposed by Okun *et al.*[44].

Pupillary dynamics also modulate functional connectivity: the percentage of statistically significant connections and 1FC group clustering coefficients is higher when computed during epochs for which pupillary size is small versus large. Supplementary Figure 7.11 C illustrates the decrease in the number of statistically significant correlations computed across 4 different quartiles of pupillary size (from low to high). The clustering coefficient distributions in L2/3 neuron L4-1FC groups are also higher when computed in the low versus the high pupillary size quartiles (as shown in Suppl. Fig. 7.11 D). In contrast, as before, the strength of the statistically significant connections in different pupil-size epochs exhibits little change (Suppl. Fig. 7.11 B). These changes may be in part due to the higher calcium aggregate activity event rates observed during the low pupil size epochs (Suppl. Fig. 7.2D). However, this is not the whole story. L2/3 neurons exhibit different modulation patterns with respect to pupillary dynamics. There appear to be *two types of modulation patterns*: the majority of neurons tend to fire at times of pupillary change, some "preferring" a decrease, while others an increase in pupillary radius. Overall our analysis suggests that L2/3 neurons with large L4-1FC groups are strongly modulated by pupillary dynamics as well as

by aggregate neuronal activity. In contrast, L2/3 neurons with small L4-1FC groups appear to be firing almost independently of aggregate measures of activity. Having said that, another question to consider is whether L2/3 neurons can be dichotomously classified as those that behave like neurons with small L4-1FC groups ("soloists") versus those that behave like neurons with large L4-1FC groups ("choroists"). Based on our measurements, this seems unlikely; rather it appears *their corresponding quartiles represent opposite ends in a continuum.*

Impact of Global Modes of Activity on Functional Connectivity

It is important to note that our findings are not particular to using the STTC measure, as we observe similar relationships when using the Pearson correlation. In particular, the overlap between the top N statistically significant functional connections estimated using the Pearson correlations and the ones identified using STTC with z-score >4 (i.e., N) is about 76% (suppl. Fig. 2.3B). Thus, our findings remain robust to the change of correlation measure.

Functional connectivity is a measure of firing synchrony, but of course, there are likely multiple causes for such synchrony. To study how aggregate population activity and pupillary modulations influence the patterns of synchrony, we applied principal component analysis on the neuronal time series and identified the principal components that explain the highest percentage of variance. Principal component analysis performed on the calcium eventograms reveals that the two dominant influences of synchronization under spontaneous conditions in the state of quiet wakefulness are: 1) spontaneous modulations in pupil size, and 2) the aggregate neuronal population activity vector (Suppl. Fig. 10A, C, e.g., see PC1 and PC2). In agreement with our observations above, L2/3 neurons with small L4-1FC group sizes tend to have smaller (absolute) weights with respect to this principal component versus neurons with larger groups (Suppl. Fig. 10B, for an example mouse, PC1). These modulation directions are not independent of each other, and in fact, they are negatively correlated with epochs of higher activity tending to occur when the pupil is small, a state indicative of reduced alertness or attention. Be that as it may, removing these principal components from the time series of each neuron, allows us to investigate patterns of synchrony due to other causes. Not surprisingly removing this major source of synchronization results in a significant decrease in the number of significant functional connections. Specifically, we found approximately 17% of previously identified functional connections remained significant, suggesting that the functional connectivity measures we described above exhibit significant influence from global modes of activity. We, therefore, re-examined our basic results by considering edges that are statistically significant after the removal of the first two principal components (Suppl. Figs. 10F-G). The results remain essentially identical as described above (Figs. 6A,6E,6D).

So far, we have discussed how neuronal ensemble firing influences the probability of firing of single neurons. However, information processing in the cortex is best regarded as occurring via the *propagation of patterns of activity from neuronal-ensemble to neuronal-ensemble.* This is explored in the next section.

L4-Group to L2/3-Group Communication

Until now we have considered the transmission of activity from L4 groups to single L2/3 neurons. Information transmission however is likely to happen from neuronal ensemble in L4 to neuronal ensemble in L2/3. L2/3-1FC groups are natural candidates for the ensemble recipients of group-to-group communication. This is supported by: **1)** their high clustering coefficients (Fig. 4H), **2)** the fact that the majority of neurons belonging to the L2/3-1FC group also exhibit significant event-triggered average (ETA) modulations with respect to the aggregate activity of the L4-1FC group (Figs. 8A and 8B), and **3)** the high overlap between their L4-1FC groups (Suppl. Fig. 9.1A), suggesting that functionally connected L2/3 neurons can in principle receive more significant shared input from L4 compared to neurons that are not functionally connected.

Activity Organization within L4 and L2/3 Neuronal Ensembles

To begin to understand how patterns of activity in L4 correspond to patterns in L2/3, we examined how L4 functional connectivity groups of different L2/3 neurons overlap with each other. Several observations were made: **1)** The degree of connectivity of L2/3 neurons in L4 correlates strongly with the degree of connectivity the neuron has in its own layer (L2 or 3; see Suppl. Fig. 4.2); **2)** L4-1FC groups of functionally connected pairs of L2/3

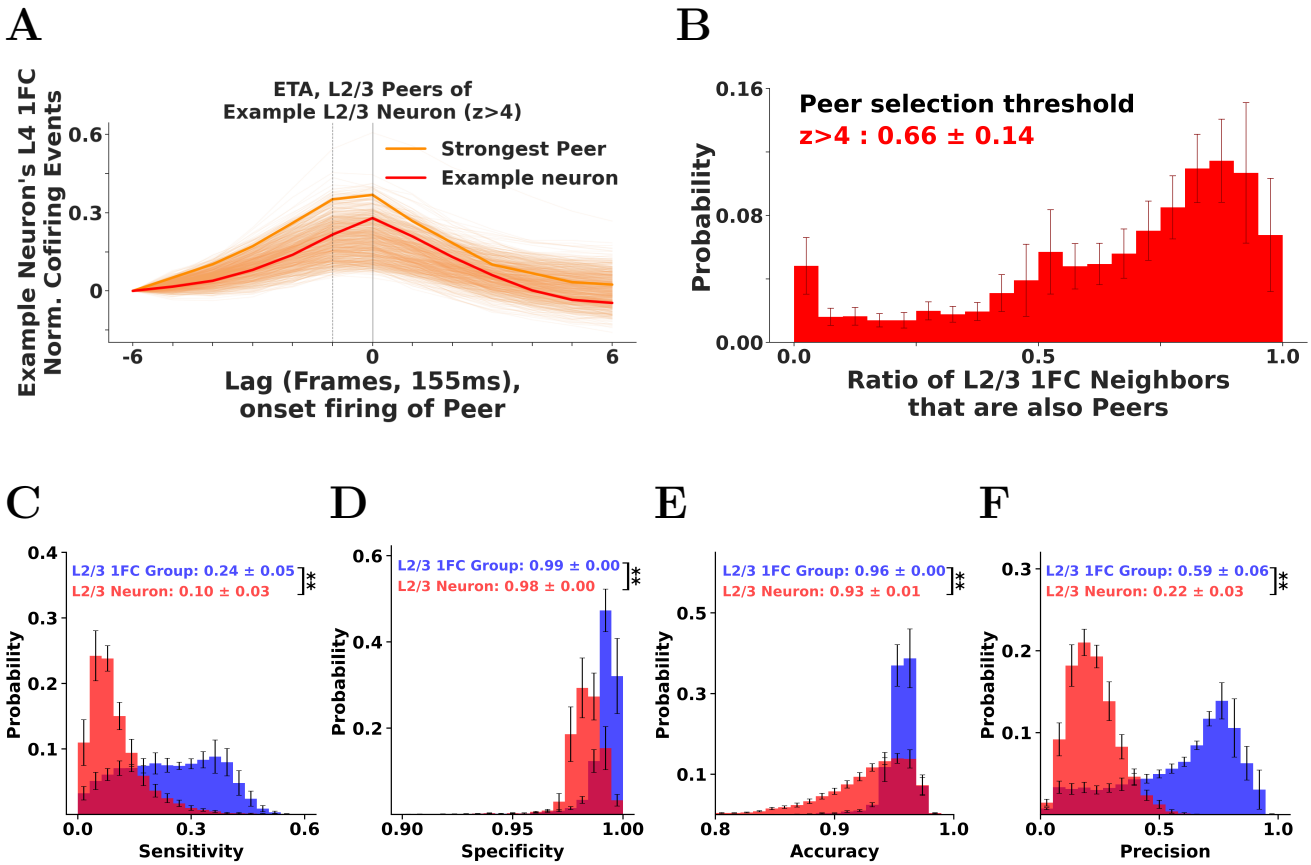

Fig. 8: **L4 Group to L2/3 Group Communication**. A) For each L2/3 neuron (say neuron R), we call another L2/3 neuron (e.g., neuron P) its *peer*, if P becomes significantly modulated as a function of cofiring events in the L4-1FC group of R. To determine that, we use the event triggered average (ETA) of P with respect to the L4-1FC group cofiring of R. We identify the peak of the ETA of neuron P and determine whether **i)** it is significantly different from the baseline L4-1FC group cofiring and whether **ii)** it occurs at lag ≤ 0 (at or before P's firing). Z-score > 4 is set as the threshold for significance. Panel A shows the ETAs of the peers of an example "reference" L2/3 neuron. Red line: the L2/3 neuron's L4-1FC group cofiring activity. Gold line: ETA of one strong L2/3 neuron peer. Other lines correspond to the remaining peers. B) Fraction of the L2/3-1FC group (L2/3 neurons functionally connected to the "reference" L2/3 neuron) that are also peers to the "reference" L2/3 neuron. For the statistical significance of the functional connectivity as well as peer identification z-score threshold > 4 was used; Note that there is a large overlap between these groups, rendering credence to the notion that they may represent ensembles of neurons involved in information transmission from L4 to L2/3. C) Let's say that the L4 1FC and L2/3 1FC groups are *active* when they exhibit *significantly large cofiring*. We measure the synchronicity of the activity of the L4 1FC group with the activity of the corresponding L2/3 1FC group vs. the firing of the L2/3 neuron. The significance threshold was chosen to be z-score>3 for the L4-1FC and z-score>2 for the L2/3-1FC group. The latter was selected in order to have the average number of frames in which the L2/3-1FC groups are active to be similar to the average number of calcium events occurring in the "reference" L2/3 neurons. This allows a more fair comparison between the transmission of information from the L4-groups to the L2/3-groups versus to the individual L2/3 neurons. Note that the results we describe below survived a sensitivity analysis we performed for other thresholds. It is reasonable to assume that activity transmission manifests at frames when both groups are simultaneously active. It is reasonable to assume that activity transmission manifests at frames when both groups are simultaneously active. Panel (C) histograms the sensitivity of the activity transmission from the L4-1FC group to the corresponding L2/3-1FC group (blue) compared to the activity transmission of the L4-1FC group to the individual "reference" L2/3 neuron (red). Sensitivity measures the fraction of frames in which the L4-1FC group is active given the L2/3-1FC group is also active. Clearly, group to group transmission has much higher sensitivity than group to neuron transmission. D) As in C) for specificity: the ratio of frames in which the L4 1FC group is inactive given the L2/3 1FC group is also inactive; Specificity is also noted to be higher for group to group transmission. E) Accuracy measures the fraction of frames where the L4 and L2/3 1FC groups are both active or inactive. F) as in C) for precision, namely the ratio of frames at which the L2/3 1FC group is active.

Fig. 8: given the L4 1FC group is also active. The standard exclusion criteria have been applied. In addition, L2/3 neurons without L4 1FC groups have not been included. Inset values indicate the mean ± standard deviation of the sample means across mice, while error bars correspond to SEM across mice (n=5). Error bars correspond to the SEM across mice (n=5); P-values: "*" < 0.05; "**" < 0.01; "***" < 0.001, "n.s.": non statistically significant. The highest p-value obtained from the permutation of means, the Welch's t-test, and the ANOVA F-test is reported.

---

neurons have greater overlap than non-FC pairs (Suppl. Fig. 9.1.A left). L4-1FC groups of functionally connected (z-score > 4) L2/3 neuron pairs have larger overlap than L4 groups of the same size of randomly selected neurons (Suppl. Fig. 9.1.A, middle). This suggests that much of the correlation in L2/3 arises from common input from L4. Moreover, the larger the group sizes of the two L4-1FC groups, the higher the overlapping as expected (Suppl. Fig. 9.1.B); **3)** The overlap between L4-1FC groups and L2/3 1FC groups of functionally connected L2/3 neurons are strongly positively correlated (Suppl. Fig. 9.1.C). **4)** The overlap between the L4-1FC groups of a pair of functionally connected L2/3 neurons does not seem to depend strongly on distance or orientation preference between the pair (Suppl. Fig. 9.1D & E, respectively); **5)** L2/3 neurons with small L4-1FC groups (putative "soloists") tend to fire independently from each other, independent of their L4-1FC group overlap (Suppl. Fig. 5.3 B). For example, 95% of the L2/3 neural pairs with small L4 groups have a probability of cofiring that is not significantly higher than the product of their firing probabilities. This argues that these groups provide a largely decorrelated channel of information transmission, at least under spontaneous conditions. **6)** In contrast, L2/3 neurons with large L4-1FC groups (putative "choristers") tend to fire in a correlated fashion (suppl Fig. 5.3, A); moreover, the larger their L4-1FC group overlap, the higher their correlation (suppl Fig. 5.3 B).

We conjecture that *information processing modules* or *pathways* operate from L4-1FC groups to L2/3-1FC and/or "L2/3-peer" groups. Let's say that the L4-1FC and L2/3-1FC groups are *active* when there is a significantly large cofiring (above a given z-score threshold; see methods and Fig. 8). Activity transmission can be considered to occur at frames where both groups are simultaneously active. A natural question to ask is whether functionally connected neurons in L2/3 act synergistically to transmit neuronal group activity in L4 more reliably. Fig. 8 and Suppl. Fig. 9.1 present information suggesting that this is the case. Specifically, Fig. 8 shows that L4-1FC group to L2/3-1FC group activity transmission has better sensitivity, specificity, accuracy, and precision compared to L4-1FC group to individual L2/3-neuron transmission. Communication from L4-1FC to L2/3-1FC groups may then be considered as an example of "ensemble-to-ensemble" transmission, capable of transmitting synchronous neuronal activity more reliably compared to L4-group to L2/3 single "unit" transmission.

3 Discussion

Resting-state connectivity analysis is an accepted method for revealing functional relationships between different brain areas and classifying brain networks that cooperate to perform important brain computations. Here we performed resting-state connectivity analysis at the level of the cortical microcircuit, focusing on the granular and supragranular layers of the mouse primary visual cortex (area V1). Understanding the functional correlation structure of the cortical microcircuit gives us a window for understanding the algorithmic structure of the computations performed by the brain that is complementary to information gained by studying anatomical connectivity.

A large body of literature has been debating the degree to which cortex strives to reach a low correlation state[27,45], favoring maximal information encoding, versus a state that retains significant correlation structure[46,47]. The weight of the evidence, including the relatively low strength of cortico-cortical pyramidal to pyramidal cell connectivity[48,49] suggests that information processing progresses by engaging multi-neuronal ensembles of pyramidal neurons to fire in close temporal proximity, cooperating with each other[50] and trading information capacity for flexibility and robustness. The rules that govern such multi-neuronal ensemble coordination remain inadequately elucidated. Here, we focused on studying neural synchronization (functional connectivity) in the absence of visual stimulation, when the brain is not engaged in a specific cognitive task. Our objective was to gain insights into the intrinsic patterns of neural activity, which provide the foundation/background on which cognitive processes are implemented.

Strength and prevalence of spontaneous pairwise inter-neuronal correlations

We identify and characterize neuronal patterns of synchrony occurring at the time scale afforded by mesoscopic large-field-of-view 2-photon imaging (∼155ms per frame). We show that, while this time scale is relatively coarse when compared to electrophysiological recordings, it remains capable of capturing several important aspects of the patterned neuronal activity permeating through cortical networks. Applying a conservative significance criterion (z-score > 4) over one hour-long spontaneous recordings yields a substantial fraction ∼14-25% of statistically significant positive pairwise functional connections between pyramidal neurons, both within and across cortical layers 2/3 and 4 in mouse area V1. The fraction of significant inter-neuronal connections is ∼12% higher within L4 (Fig. 2G,4E), the main recipient layer of thalamocortical projections, suggesting a degree of decorrelation occurs as information travels from L4 to supragranular layers.

The observed statistically significant correlations are not uniformly distributed. Instead, the fraction of significant positive correlations peaks near the location of the soma but then falls gradually, extending over relatively large distances, at least up to ∼1.2mm, the largest distance considered here. The rate of fall with distance appears to be slightly faster in L2/3 compared to L4 (Fig. 2C, 2F). The decrease in probability of positive functional connectivity with distance is in agreement with reports from the literature which suggest that anatomical connectivity similarly drops with distance from the soma[33,51]. Compared to positive correlations, anticorrelations are weaker and more difficult to detect given the relatively low firing rate of the neurons. Nevertheless, we identified ∼5%, 7% and 7% significantly (z-score < -2) anti-correlated functional connections in L4, L2/3, and L4 → L2/3 respectively, whose density tends to peak ∼600μm away from the soma (Suppl. Fig. 2.8 A,C). This argues that functional connectivity within and across cortical layers maintains a loose center-surround organization, with positively correlated units clustering around the soma, while negatively correlated ones typically found ∼0.6 mm away.

Neurons that fire together wire together; multiple studies have demonstrated increased anatomical and physiological connectivity between pairs of neurons with similar tuning properties[29,33,34]. Here, too we were able to demonstrate an increased percentage of significant positive functional correlations among pairs of neurons with similar orientation/direction tuning properties or high receptive field similarity (Figures 3B, 3D). Conversely, anti-correlated functional connections were more common among neurons with perpendicular orientation tuning, especially in L2/3 (Suppl. Fig. 3.1). However, it is important to point out that these relationships are relatively weak, as functional correlations appear to be rather promiscuous with regard to the properties of the pairs of neurons they connect (Figure 3B). This is especially true in L4 (Fig. 3B, left panel). Overall, a considerable fraction of significant functional connections occur between neurons with disparate tuning functions, suggesting that activity patterns observed under spontaneous conditions would not be expected to necessarily recapitulate the signal correlations seen in the presence of stimuli.

Although a sizeable fraction of pairwise functional correlations reach significance, on average the pairwise correlation coefficients we measure are small (0.01-0.02, Fig. 2A, D), commensurate to prior reports suggesting that noise correlations are low in the visual cortex[27,46]. Even among pairwise functional correlations that reach significance, correlation strengths remain distributed around relatively low correlations values (∼mean 0.053±0.004 for L4 (Fig. 2H). The shape and center of this distribution remain consistent within and across layers (Figs. 2A, 2D,2H), its tail towards high correlation values rarely (0.1%) exceeding 0.15. Therefore, even when it reaches significance, pairwise functional connectivity among pyramidal neurons remains weak, in agreement with reports of weak physiological connectivity among excitatory units in mouse area V1[48,49]. This is true across cortical layers as well as a function of inter-neuronal distance, underscoring the fact that this represents a cortical circuit connectivity principle. Notably, little pairwise correlation strength is needed to generate significant cofiring events among large aggregates of neurons[47]. A simple neuronal population model with mean firing rates commensurate to the ones we observed, shows that highly statistically significant cofiring events can be generated even when pairwise correlations remain low (Suppl. Fig. 2.9, related suppl. text). These observations reaffirm the concept that large ensembles of neurons need to be synchronized in order to effectively transmit their state of activation downstream and show that this can occur in the setting of very weak pairwise correlations. Maintaining the strength of pairwise correlations at low levels in cortical circuits is not accidental; rather it is likely to reflect a universal principle shaped by circuit normalization processes that include contribution from inhibitory elements. In general, weak and promiscuous pairwise neuronal correlations may be advantageous for addressing efficiently the tradeoff between information capacity and ability for fault-tolerance, network flexibility, and generalization.

It is important to note that, although the absolute number of significant correlations may differ (Fig. 4E), the basic observations we report here are robust to reasonable changes of the measures we use for identifying significant

functional correlations. Specifically, they are robust with respect to: **i)** the choice of significance threshold z-scores, **ii)** the choice of the measure used for measuring correlations, i.e. Pearson or STTC (Suppl. Fig. 2.3 B), or whether the time interval chosen for the STTC definition (Δt) corresponds to 0, 1 ($\sim$150ms) or 2 frames ($\sim$300ms) (Suppl. Fig. 2.1), and finally **iii)** the choice of the duration of imaging (as long as it is sufficiently long; suppl. Fig. 2.2). Suppl. Fig. 2.2B demonstrates that our ability to detect significant correlations is strongly and inversely related to the duration of imaging: for example, upon restricting the duration of analysis to 15-minute intervals only approximately 5% significant positive correlations are identified in L2/3, compared to $\sim$14% when using the full 60-minute duration (suppl. Fig. 2.2B; a similar fractional difference is also seen in other layers). Conversely, >80% of edges identified as significant in any 15-minute interval are also significant when considering the full 60-minute duration (Suppl. Fig. 2.5 "Entire"). Requiring functional connections to be significant in all non-overlapping 15-minute intervals tends to select connections that are both statistically significant during the entire recording and exhibit larger connectivity strength, and may therefore identify a *core*, more robust, network of functional connectivity. For example, functional connections in L4 identified as statistically significant during *all* 15-minute intervals did exhibit stronger bias in orientation preference than other connections (Suppl. Fig. 4.6B). In contrast, functional connectivity relations that come and go may reflect a *more flexible component* of the functional connectivity network. Studying how the structure of functional connectivity networks changes in different brain states or after training in different types of cognitive tasks would likely be a fruitful endeavor for future research, though outside the scope of the current manuscript.

Structure of functional connectivity architecture in granular and supragranular layers

The first-order functional connectivity group (1-FC) of a pyramidal neuron ("index" neuron) represents a natural definition for the "minimal" neuronal ensemble with which the neuron "cooperates" to process cortical patterns of activity. It is therefore well-worth investigating the architecture and properties of these ensembles in relation to the properties of their constituent neurons. In a sense, this takes a first step in moving away from single units to studying how neuronal ensembles cooperate in processing patterns of activity. An argument in support of this claim is that 1FC groups exhibit excess correlations, even after one controls for correlations contributed by the epochs of firing of the defining member of the group ("index" neuron). Fig. 4B, H show that clustering coefficients calculated after removing epochs of firing of the "index" neurons are strikingly shifted to the right (means of 0.45-0.55) compared to the null (control, means of 0.12-0.22) distributions for all categories of 1FC groups analyzed. Interestingly, the distribution of clustering coefficients in L2/3 is shifted slightly to lower values compared to that within L4 as well as across layers (1FC groups generated in L4 from index neurons in L2/3). This argues that 1FC groups in L4 may be more internally interconnected and multiplex less with other groups that have distinct functions.

The degree of connectivity is an important parameter that influences network function[52–54]. Fig. 4A histograms the degree of connectivity of pyramidal neurons within and across granular and supragranular layers. The probability of finding neurons with a given degree of connectivity drops rapidly as a function of degree in layers 2 and 3 as well as for inter-layer connectivity (L4 to L2/3). In contrast, the distribution of intra-L4 degrees of connectivity appears to be more uniform and extends to higher degrees of connectivity (Fig. 4G). Networks whose degree of connectivity distribution follows a power law are scale-free and manifest robustness to random failures[52]. Power-law trends in the degree of connectivity imply lack of internal scale, so that nodes with widely different degrees coexist in the same network and can give rise to emergent behaviors. Although it comes close, the functional form of the observed distributions does not necessarily conform exactly to a power law (Suppl. Figure 4.1, especially for L4 and L3). Overall L4 conforms best to a linear fit (uniform distribution) up to 0.45 (fraction of neurons in the field of view), followed by a sharp decay in the tail, while L2/3 conforms best to an exponential fit. In any case, networks in all layers exhibit substantially higher robustness compared to corresponding theoretical (control) networks, namely Erdős–Rényi and regular ring graphs with the same average degree of connectivity. This is reflected in their corresponding higher Molloy-Reed indices (ratio of the mean squared degree of connectivity to the mean degree of connectivity; see[52,55,56]), which are generally much higher and well above 2 (see Methods; Suppl. Fig. 4.9B). Interestingly, L4 exhibits a higher degree of robustness than L2 and L3 (see Suppl. Fig. 4.9B) to go with the fact that its degrees of connectivity extend to higher values and are more uniformly distributed. The uniform degree of connectivity structure allows for a more balanced occurrence of L4-1FC group sizes and may be advantageous in processing efficiently input signals containing features that require equiprobable representation over a

range of scales. This structure has also implications for robustness since the loss of any single node has a limited impact on the overall connectivity.

Small-world network architecture is an important concept in neuronal circuitry[57,58], as it preserves efficient information processing while optimizing the trade-off between local modularity and specialization versus global integration. The functional networks in each layer we examined exhibit "small-world" properties (Suppl. Fig. 4.8). All layers have 1-FC groups with relatively high clustering coefficients and very short paths between them, which supports the effective integration of multiple segregated sources of information. In each layer, the estimated average shortest path considering all neuronal pairs is about 2 (Suppl. Fig. 4.8C-D), which is close to $\ln(\ln N)$, where N is the total number of neurons at that layer and smaller than what is expected for regular random graphs[25,52]. The spatial topology of functional connectivity in L4 and L2/3 bears resemblance to the "local plus uniform" model[59], in which a portion of connections is local and another one between randomly chosen units is uniformly distributed (with less than 10% long-range connections) irrespective of their metric distance. This type of network exhibits high clustering coefficients, facilitating modularity, as well as short paths, facilitating communication between modules and long-range functional integration. This favors network scalability and overall efficiency while affording acceptable fault tolerance and easier network expansion.

Dependence of functional connectivity on brain state

Functional connectivity is not a fixed property of neural circuitry; rather it can be modulated by multiple factors including engagement in different cognitive states. To study the dependence of functional connectivity on the physiological state of the animals, we employed two surrogate measures, namely pupillary size modulation and aggregate neuronal population firing activity. These measures are not necessarily independent from each other; in fact, they are negatively correlated, as epochs of small pupil size tend to have larger aggregate population activity, likely because they reflect states of reduced alertness and lower sympathetic response. As reported previously[42,60], these conditions favor both increased firing rate and higher correlations. This is corroborated here, as the fraction of significant functional connectivity edges computed over epochs of small pupil size (0-25% quartile) is more than double that computed over epochs of high pupillary diameter (75-100% quartile; Suppl. Fig. 7.11C). In conjunction with the overall pairwise connectivity increase, the degree of connectivity and clustering coefficients of 1FC groups (Suppl. Fig. 7.11D) also shifts to the right suggesting an increase in neuronal cooperativity during epochs of small pupil size. Similarly, during epochs of high aggregate activity, the fraction of significantly connected pairs markedly increases (Suppl. Fig. 7.4A) together with the right shift in the degree of connectivity and clustering coefficient distributions (Suppl. Fig. 7.4B).

Another surrogate marker indicative of different brain states is the status of locomotion. We repeated the above analysis incorporating only frames in which the animal was walking, and found that cortical networks exhibit increased decorrelation, which results in a smaller number of statistically significant edges, degree of connectivity, and clustering coefficient, compared to equal durations of a randomly selected interval of quiet wakefulness, where mice were not locomoting (Suppl. Fig. 11.2). It is worth pointing out that, in contrast to the relatively strong modulation of functional correlation significance by brain state, the *functional connectivity weight distribution remains centered around small correlation values and changes little, if at all*, across different aggregate activity or pupillary size quartiles (Suppl. Figs. 7.5B, 7.11B). This further reinforces the point that the *magnitude of functional correlations is tightly regulated in the cortex.*

Implications for inter-laminar information transmission

Information processing in the cortex is best viewed as the result of activity pattern transmission from neuronal ensemble to neuronal ensemble. Functional connectivity analysis under spontaneous conditions gave us the opportunity to identify putative neuronal ensembles that participate in the information "handshake" that occurs between cortical layers in the absence of external stimulation. Specifically, we studied the relation between patterns of activity emerging in L2/3 relative to patterns of activity seen in L4.

Prediction of L2/3 pyramidal neuron responses from their cofiring functional partners in L4

Of particular interest are the 1FC groups of L2/3 neurons in L4, which can be interpreted as their putative feed-forward input neurons. Following this assumption further, it is reasonable to ask how well synchronous co-firing

among the L4-1FC neuron group functionally connected to an "index" L2/3 neuron can predict the probability of firing of that neuron. Given the coarse temporal graining that 2-photon imaging affords, we focused on prediction of firing occurring within the same imaging frame (∼155 ms). We found that the probability of firing of most L2/3 neurons is well-fit by a ReLU function on the number of cofiring events occurring in their L4-1FC group during the same imaging frame, reaching certainty for some neurons (Fig. 5A, 5C). Although this is at a level of functional correlations and does not necessarily reflect a causal relationship, it is reassuring, as the ReLU activation function has well-described computational advantages including efficiency, robustness to small input changes while permitting sparsity and allowing the implementation of non-linear computations[61–64]. Choosing L2/3 neurons with good R^2 fits ($R^2 \geq 0.8$), we were able to extrapolate that the median number of cofiring events needed to strongly drive L2/3 pyramidal neurons is ∼51 (Fig. 5E), roughly commensurate to prior estimates made in a different context by Shadlen and Newsome[40].

Interestingly, at the individual neuron level, the slopes of L2/3 neuronal responses as a function of their L4-1FC group cofiring level differed markedly from each other. In particular, the slope of L2/3 pyramidal neuron response functions was inversely related to the size of their L4-1FC group, being shallower for neurons with large L4-1FC groups and steeper for neurons with small 1FC-L4 groups (Fig. 6D). It is important to point out that this was not the effect of a sampling bias that might have arisen, for example, if small groups represent sub-sampling from larger groups only a fraction of the neurons of that happen by chance to reside in the imaging layer (Suppl. Fig. 5.6, 7.9, 7.6). Rather, it appears to identify L4 to L2/3 ensemble pathways with different properties demonstrable along several dimensions. Specifically, L2/3 neurons with small L4-1FC groups tend to fire independently from the aggregate population activity (Fig. 7A, B, in light orange) thereby appearing akin to the "soloists" proposed by Okun *et al.*[44]. In contrast, neurons with large L4-1FC group sizes are strongly modulated by aggregate population neuronal activity (Fig. 7A, B, in darker colors), akin to Okun *et al.*'s "choristers". L2/3 neurons with small L4-1FC groups are also less influenced by pupillary-size modulations (Fig. 7G, suppl Fig. 7.12). Their firing rates remain "stable", independent of the aggregate neuronal activity (Suppl. Fig. 7.2A) and pupil size (supp. Fig. 7.2 C), in contrast with the firing rates of L2/3 neurons with larger L4-1FC sizes, which behave differently (Suppl. Fig.7.2 B,D). Furthermore, the slope of the response functions of L2/3 neurons with small L4-1FC groups remains invariant across epochs of different aggregate activity or pupillary sizes (Suppl. Figs. 7.7A,B, respectively), suggesting they may be able to transmit process information independent of these parameters. Although it is clear that L2/3 neurons with large versus small L4-1FC groups differ along several dimensions, it is important to point out that this classification is not dichotomous but part of a continuum including neurons with intermediate group sizes and properties. Interestingly, the spatial extent of the small versus the large groups does not differ substantially (Suppl. Fig. 5.7), so differences in group size do not simply correspond to differences in the scale of the area from which the groups integrate information in the visual field. Furthermore, no notable distinction was observed in the distribution of L2/3 neurons exhibiting consistent orientation preference between groups with large and small L4-1FC groups. Similarly, no prominent disparity was identified in the distribution of L2/3 *visually-responsive* neurons. We speculate that the balanced wide distribution of L4-1FC group sizes may be advantageous for an efficient variable-size representation, capable of encoding input patterns occurring at different scales containing variable amounts of information and required precision.

It is important to understand how L2/3 responses depend on the statistics of L4-1FC group cofiring events under spontaneous conditions, as this characterizes the baseline state of granular to supragranular layer communication in the brain. We found that the response probability of L2/3 neurons plotted against the cumulative probability of cofiring event size in their L4-1FC groups (Fig. 5G,5H) typically exhibits a sharp upward turn at a high value, indicating that L2/3 neurons tend to fire for cofiring events higher than the ∼93 percentile on average (Fig. 5I). This relatively high threshold value is narrowly distributed (Fig. 5I) across neurons and depends only weakly on L4-1FC group size, corresponding to somewhat different cofiring percentage of cells in small (cofiring percentile at threshold is ∼95%, corresponding to ∼21% of L4-1FC group cells firing) compared to the large (cofiring percentile at threshold is ∼90%, corresponding to ∼10% of L4-1FC group cells firing) groups (Suppl. Fig. 5.8). This maintains a sparse pattern of firing in L2/3 under spontaneous conditions, as L2/3 neurons engage only for ∼7-8% of the largest cofiring events occurring in their corresponding L4-1FC groups.

The fact that L2/3 neurons with small L4-1FC groups achieve the same probability of firing with fewer cofiring events in their group (Fig. 6D) argues that functional connections from small L4-1FC groups to their "index" L2/3 neuron should be expected to be stronger. However, we observed in fact the converse: namely, the distribution of STTC weights is shifted to slightly lower values for L2/3 neurons with small L4-1FC groups compared to neurons with large ones (Suppl. Fig. 5.2). On the face of it, this may seem paradoxical, but one way that it can be explained

is through multiplexing. It is important to realize that functional connectivity strength does not always equate with actual (physiological) connectivity strength. Despite being physiologically strongly connected to a pathway, a neuron may nevertheless exhibit weak functional connectivity with this pathway, if, for example, a substantial fraction of its spikes are triggered by inputs from other, not necessarily recorded pathways. L2/3 neurons with small L4-1FC groups have high firing rates and tend to fire independently from the population activity. They may therefore be *more susceptible to multiplexing with various independent pathways* compared to neurons with large L4-1FC groups, which tend to phase lock to aggregate neuronal activity and pupil size modulations.

One might wonder about the degree to which the overall number of cofiring events in a neuronal ensemble is in fact the major factor relaying information, versus the alternative of retaining information about the identity of which particular neurons fire per frame. Although it is beyond the scope of the paper to definitively prove this here, retaining identity information contributes little in addition to the information carried by the aggregate cofiring events within L4 -1FC groups. Specifically, the accuracy of the prediction of L2/3 pyramidal neuron responses was not significantly improved when the entire vector indicating the state of each L4-1FC neuron is included in addition to the number of cofiring events in each L4-1FC group. This observation was tested using an SVM classifier with linear kernel, but also random forest, Naive Bayesian, and logistic regression classifiers (see Suppl. Figure 5.4) and appears to be robust. In this study, we trained a Support Vector Machine Classifier with a linear kernel to forecast the L2/3 firing patterns of individual neurons in three distinct scenarios. The variability among these scenarios lies exclusively in the input parameters. These inputs are: i) the count of co-firings of the group of L4-1FC neighbors at a give frame, ii) the count of co-firings of the L4 (inter-) and L2/3 (intra-) layer 1FC neighbors at a given frame, and iii) the complete vector containing the IDs of its L4-1FC neighbors along with their corresponding events (firing or silence) at a given frame. Notably, the third case incorporates not only the *count of co-firing events* but also utilizes the IDs of the neurons that are firing. We compared their performance, in terms of sensitivity, specificity, and accuracy, and showed that including information about the neuron ID does not improve the performance. This is the reason we primarily focused on the analysis of ***aggregate cofiring events*** in this manuscript.

Dependence on the time scale used for computing the functional connectivity maps

L2/3 neuron activity prediction depends on the functional connectivity maps that define the L4-1FC putative input groups and is influenced by the time intervals used to compute them. As discussed above, the shorter the intervals, the stronger the pairwise correlations (STTC weights) of the statistically significant connections, the lower the number of statistically significant connections, and the smaller the degree of connectivity (Suppl. Figs. 2.2, 2.5, 4.5). We compared predictions from functional connectivity maps computed over the full 60 minutes to maps computed over non-overlapping 15-minute intervals. Despite their smaller size, L4-1FC groups computed over 15 minutes are more effective in predicting the activity of their "index" L2/3 neuron compared to 60-minute L4-1FC groups, achieving a higher L2/3 firing probability for the same number of cofiring events (Suppl. Figure 5.5). This suggests that the functional connections that rise to significance over smaller time intervals may form a stronger "core" functional connectivity network, reflecting patterns of synchrony that occur more frequently and may therefore be more essential for cortical processing under spontaneous conditions. We speculate that this architecture, which consists of core networks of neuronal ensembles which contain a fraction of more loosely functionally-connected members may be particularly beneficial for learning as it has the capacity for multiplexing to learn new patterns while preserving the pre-existing information structure.

Efficient information transmission takes place from neuronal ensemble to neuronal ensemble

Information transmission is likely to proceed from neuronal ensembles in L4 to neuronal ensembles in L2/3[1,4,40,65] rather than from ensembles to isolated, individual, neurons. We investigated whether functionally connected ensembles of neurons we identified could serve as such "pathways" for information transmission[50]. A natural candidate as a recipient of information propagating from L4 to L2/3 are the intra-layer L2/3 functional connectivity groups formed by each L2/3 neuron. As we showed, these groups have high clustering coefficients (Fig. 4H) suggesting they tend to fire synchronously. Furthermore, the L4-1FC groups of their constituent neurons exhibit much higher overlap than expected by chance (Suppl. Fig. 9.1.A), suggesting they share significant (putative) common input from L4. This is further corroborated by the significant peaks exhibited in the event-triggered averages of a L2/3 neuron's L2/3-1FC group members, with respect to the aggregate cofiring activity of the neuron's corresponding

L4-1FC group (its putative input; Fig. 8A and 8B). We could therefore ask whether L2/3-1FC neurons act synergistically to "receive" L4 cofiring events more reliably than single L2/3 pyramidal neurons, when both are modulated by their common L4-1FC "putative input" neuronal ensembles. In order to gauge this, we computed the sensitivity, precision, and specificity with which synchronous activity in the L4-1FC "putative input" groups predicts the level of cofiring activity in the corresponding L2/3-1FC connectivity groups, compared to the probability of firing in the corresponding individual L2/3 neurons (Fig. 8C-8F). Care was taken to ensure a fair comparison, by setting the threshold of L2/3-1FC group cofiring so that, on average, the number of imaging frames where the group was deemed to be active was equal to the number of frames where "index" L2/3 neurons had firing events and by doing a sensitivity analysis at nearby thresholds. Fig. 8C-8F show clearly that ensemble to ensemble "information" transmission to the L2/3-1FC groups is both more sensitive and more specific than ensemble to single unit transmission. This group-to-group transmission of information is consistent with the existence of *pathways* discussed in Smyrnakis *et al.*[50]. These pathways are groups of neurons that stochastically transmit information associated with the particular choice of neurons. In Smyrnakis *et al.*[50] it is shown that, under reasonable assumptions and provided that pathway neurons do not cover the space too densely, there is a definite network capacity advantage. The increased information capacity is due to the ability of multiple non-interfering pathways to coexist.

We found that L2/3 neurons, modulated by common L4 ensembles act synergistically to transmit the activity more reliably than in the case of single neurons as reflected by the sensitivity, precision, and specificity that compare the synchronicity of the activity of the L4-1FC group with the activity of the corresponding L2/3 peer group vs. the firing of the L2/3 neuron. In sum, under spontaneous conditions, we were able to identify a mode of information transmission from L4 neuronal ensemble to L2/3 neuronal ensemble that appears to be more reliable than L4 ensemble to L2/3 neuron transmission. These ensembles are reminiscent of neuronal ensembles identified by Carrillo Reid *et al.*[66] using different criteria. In the future, the analysis of the behavior of these ensembles under causal optogenetic manipulation as well as stimulus presentation conditions, will shed further light on the information processing machinery of the visual cortex.

Limitations of our study

We have not tried to relate spontaneous patterns to stimulus-induced patterns of activity. Deciphering the relationship between spontaneous and elicited patterns of activity is an important line of research to follow, as it has been argued[14] that spontaneous activity patterns recapitulate in part patterns of sensory activation. The temporal resolution of 2-photon calcium imaging is limited and our imaging frame rate is ∼155ms. Therefore, the functional connectivity we measure has limited temporal resolution. This is the reason that we considered the STTC measure at $\Delta t = 0$, sensitive to synchrony within the same image frame of duration ∼155 ms. We do not have the temporal resolution to resolve patterns of activity faster than that, making it difficult for example to separate feed-forward influences from L4 to L2/3 versus indirect inputs or backward projections from L2/3 to L4. Be that as it may, it remains informative to ask how well the level of cofiring in the L4-1FC group of L2/3 neurons can predict whether the L2/3 neurons fire a calcium event within the same imaging frame. It is also encouraging that when we broaden the temporal resolution window of the functional connectivity analysis to $\Delta t = 2$ imaging frames, we observe the expected asymmetry in directional functional connectivity links (see Methods), with more directional links arising from L4 to L2/3, i.e., along the feed-forward projection, rather than in the opposite direction (Suppl. Fig. 2.1). It is important to point out that we did not intend to infer causality from the observations outlined above. Even if we applied other techniques, like Granger causality, the temporal resolution of the calcium imaging would remain a limiting factor in dissecting causal relationships within the cortical microcircuit. Nevertheless, neuronal ensembles that fire in synchrony remain highly relevant for information transmission in the brain[67], even within the relatively coarse time-window afforded by calcium imaging (here ∼155ms). Identifying the patterns of synchrony elicited during epochs of spontaneous activity yields information about the structure of the circuit that underlies the computations the visual cortex is designed to perform.

4 Conclusion

We had several key findings: **1)** A substantial number of statistically significant positive pairwise neuronal correlations exists within area V1 Layers 2, 3, and 4, some of which are reasonably long-range (up to 1 mm), more prominent within L4. Anticorrelated functional connections are weaker and appear to be more spread out spatially, peaking on average at larger distances from the "index" neuron. Overall, there is little difference in the

distribution of pairwise correlation strengths between pyramidal neurons under various conditions, suggesting that it represents a relatively conserved property of cortical microcircuits.

2) The "hub" structure differs across layers. In layers 2/3, the fraction of neurons with a given degree of connectivity falls as the degree of the connectivity rises, whereas in L4, it remains approximately flat until much higher values. This uniformity suggests L4 networks have less of a hierarchical structure, achieving a more even distribution of the computational load across the nodes, shorter path lengths, and better fault tolerance and robustness. In contrast, L2/3 networks exhibit a more hierarchical structure, promoting efficient computations and network scalability. Furthermore, balanced connectivity may allow the L4 network, which is the chief recipient of input from the lateral genicular nucleus, to learn to process more effectively a wider-range of input patterns, before passing on the information to L2/3. Both layers exhibit robustness and "small-worldness".

3) Going beyond pairwise correlations, we identified first-order functional connectivity neighborhoods that act as "cooperative" multi-neuronal units, potentially serving as computational modules. L4-1FC group cofiring predicts the probability of calcium events in its corresponding L2/3 neurons. Interestingly the size of the L4-1FC group affects the slope of the prediction function, with smaller L4-1FC groups showing steeper responses, implying they exhibit increased efficacy in transmitting synchronous activity downstream from L4.

4) The probability of firing of L2/3 neurons rises monotonically as a function of cofiring events occurring within their L4 1FC (putative input) group. Their response function exhibits two regimes, characterized initially by a weak response followed by an approximately linear fast-rising phase, which starts approximately when 13% of the L4-1FC group neurons fire. L2/3 neurons tend to remain silent for the majority (92%) of cofiring events occurring within their L4-1FC groups.

5) Information transmission may be best viewed as occurring from neuronal ensembles in L4 to neuronal ensembles in L2/3. Under spontaneous conditions, we were able to identify a mode of information transmission from L4-1FC groups to L2/3-1FC groups that appears to be more reliable (has better sensitivity, precision, specificity) than L4-1FC group to L2/3-neuron transmission.

6) Internal state modulations, as evidence by pupillary size changes or changes in aggregate neuronal activity, do influence functional connectivity. Epochs of high aggregate activity and small pupil size tend to yield a higher number of significant pairwise functional connections.

7) Neurons exhibit distinct properties based on their functional connectivity group sizes. L2/3 neurons with a relatively small number of functional connections in L4 are weakly, if at all, modulated by changes in pupil size or aggregate population dynamics, and tend to fire independently from one another. In contrast, L2/3 neurons with a large number of L4 connections are strongly modulated by changes in pupil size or aggregate population dynamics and tend to correlate with each other.

8) The central trends we describe here were robust to changes in functional-connectivity measure. They were also robust to the removal of the first two principal components of neuronal activity, which are strongly correlated with aggregate population activity and pupil size.

In the future, functional connectivity analysis of cortical microcircuitry could be used to study the communication between brain areas in the presence or absence of sensory stimulation as well as changes that occur during different perceptual states and learning. Causal analysis and manipulation of neuronal ensembles identified in the process could help set the foundations for understanding the principles of multi-neuronal information processing in both health and disease.

5 Material and Methods

Experiments and Data Collection

Mouse Lines and Surgery All procedures are approved by the Institutional Animal Care and Use Committee (IACUC) of Baylor College of Medicine. 5 mice, 0-12 weeks of age, expressed GCaMP6s in excitatory neurons via SLC17a7-Cre and Ai162 transgenic lines (JAX stock 023527 and 031562, respectively) cross. Animals were anaesthetized and a 5 mm craniotomy was placed over visual cortex. Each mouse recovered for $\sim$ 2 weeks prior to the first experimental imaging session.

2-photon Imaging Mice were head-mounted on a treadmill and calcium imaging was performed using Chameleon Ti-Sapphire laser (Coherent) tuned to 920 nm and a large field of view mesoscope (ref) equipped with a custom objective (0.6 NA, 21mm focal length). Laser power after the objective increased exponentially as a function of depth from the surface according to: $P = P_0 \times e^{(z/Lz)}$, where P is the laser power used at target depth z, P_0

is the power used at the surface (not exceeding 15mW), and Lz is the depth constant (not less than 220μm.) Maximum laser output of 90 mW was used for scans approximately 450 μm from the surface and below.

Monitor Positioning and Retinotopy Visual stimuli were presented to the left eye with a $31.1 \times 55.3 cm^2 (h \times w)$ monitor (resolution of 1440 × 2560 pixels) positioned 15 cm away from the mouse eye. Pixelwise responses across $2400 \times 2400 \mu m^2$ to $3000 \times 3000 \mu m^2$ region of interest (0.2 px/μm) at 200-220μm depth from the cortical surface to drifting bar stimuli were used to generate a sign map for delineating visual areas Garrett, 2014 #1018. We chose an imaging site spanning all primary visual cortex visible within the craniotomy and a fraction of the adjacent medial and lateral higher visual areas. Imaging was performed at $\sim$ 6 Hz for all scans, collecting eight scanfields at 0.6 px/μm xy-resolution to tile a cortical column (1 field per layer at depths XX). Across 2-5 sessions, a scan was collected at each target depth by manually matching reference images to target depth within several microns using structural features including horizontal blood vessels (which have a distinctive z-profile) and patterns of somata (identifiable by GCaMP6s exclusion as dark spots). Imaging data were motion-corrected, automatically segmented and deconvolved using the CNMF algorithm[21]; cells were further selected by a classifier trained to detect somata based on the segmented cell masks. This resulted in $\sim$ 7000-8000 soma masks per animal per column.

Directional Visual Stimulus A stimulus using smoothened Gaussian noise with coherent orientation and motion was used to probe neuronal orientation and direction tuning. An independently identically distributed (i.i.d.) Gaussian noise movie was passed through a temporal low-pass Hamming filter (4Hz) and a 2-d Gaussian filter ($\sigma = 4.4°$ at the nearest point on the monitor to the mouse). Each scan contained 72 blocks, with each 15-second block consisting of 16 equally distributed and randomly ordered unique directions of motion between 0-360 degrees with a velocity of 42 degrees/s at the nearest point on the monitor. An orientation bias perpendicular to the direction of movement was imposed by applying a bandpass Hanning filter G(ω; c) where ω is the difference between the image 2d Fourier transform polar coordinates ϕ and trial direction θ, and

$$G(\omega; c) = \sqrt{c} H(c\omega)$$

$$H(\omega) = \begin{cases} \frac{1}{2} + \frac{1}{2}\cos\omega & \text{if } |\omega| < \pi \\ 0 & \text{otherwise} \end{cases}$$

Here, c = 2.5 is an orientation selectivity coefficient. The resulting kernel is 72° full width at half maximum.

Direction/Orientation selectivity. The directional trial response was measured by taking the difference in cumulative deconvolved activity at the linearly interpolated trial onset and offset time points. Trial responses per direction were modeled as a two-peak scaled von Mises function in the form:

$$\upsilon = a_0 + a_1 g(\phi) + a_2 g(\phi - \pi),$$
$$g(\phi) = \exp(-w(1 - \cos(\phi - \theta)))$$

where θ is the preferred direction, ϕ is the trial direction, w is the peak concentration, a_0 is the baseline, and a_1, a_2 are the independent amplitudes of two peaks. The two peaks share a preferred orientation, baseline, and width, but their amplitudes are fit independently. This function was fitted to minimize the mean squared error of all trial responses across 16 directions using the L-BFGS-B optimization algorithm (ref-new). Significance and goodness of fit were calculated by permutation. Trial direction labels were randomly shuffled among all trials for 1000 refits. The goodness of fit was calculated as the difference in fraction variable explained (FVE) between the original fit FVE and the median FVE across all 1000 shuffled fits. The p-value was calculated as the fraction of shuffled fits with a higher FVE than the original fit. Neurons were included for further network analysis if p-value < 0.001 and the difference in FVE was > 0.025.

The neurons' orientation and direction tuning were estimated as in Fahey *et al.*[37]. Briefly, responses to a dynamic stimulus of pink noise with coherent orientation and motion were fit with a two-peak von Mises function. Cells were included for further analysis by a dual threshold for the fraction of variance explained (>2.5%) and significance calculated by permutation $p \leq 0.001$. In our sample, $\sim$46% of L4 neurons (2081 out of 4551) and $\sim$50% (7349 out of 14774) of L2/3 neurons were orientation selective using these criteria, in agreement with[37]. All orientation selective units were then sorted "cyclically" into 128 bins according to the preferred direction of the larger amplitude von Mises peak. The cells that are oriented have p-value ≤ 0.001 and FVE > 0.025.

Absolute Orientation Difference For each pair of neurons (n1, n2), we estimate the absolute direction difference of their strongest amplitude angle w1 and w2, respectively, ϕ as follows:

$$\phi = min\{|w1 - w2|, 360^\circ - |w1 - w2|\}.$$

The corresponding absolute orientation difference ω of their strongest amplitude is equal to ϕ, for ϕ equal or less than 90° otherwise, it is equal to $180^\circ - \phi$.

Receptive Field Structure and Similarity Receptive field maps were calculated using spike-triggered pixel-wise average (STA) of the monet movie frames preceding the spike event in the neuron by 250 ms (spike-triggered activity integration window [-250 0] ms). The resulting STA maps were filtered with 2d Gaussian filter using 10 * 10 pixels kernel. The maximum response location was set within the 95% of the Gaussian fit amplitude (receptive field region of interest (RF ROI)). Signal-to noise ratio (SNR) was determined as a ratio of variance within the receptive field ROI and variance of the background (all pixels of the map outside Gaussian fit for the receptive field). Only cells with SNR≥2 were considered to have defined visual receptive fields and accepted for further analysis. For accepted cells (SNR≥2), the STA maps were converted to z-score maps (using map mean and standard deviation to assign z-score to every pixel). Next, the values [-2 2] were set to 0. For the resulting maps, we calculated the pairwise structural similarity index (SSIM[68]), indicative of the 2d-correlation between the on- and off-field structure of the two maps. Next, we explored the relationship between SSIM and STTC values between neurons.

Software Experiments and analyses were performed using custom software developed using the following tools: ScanImage, CaImAn, DataJoint[69,70], PyTorch[71], NumPy[72], SciPy[73], Docker, matplotlib[74], cmocean, Jupyter, pandas[75,76], scikit-learn[77], multiprocessing.

Deconvolution The fluorescence signal recorded through two-photon microscopy from neurons is deconvolved to obtain an estimated spike train as described in Pnevmatikakis *et al.*[21]. The neurons recorded express the GCaMP6s indicator. The Pnevmatikakis *et al.*[21] method simultaneously identifies individual neurons, demixes spatially overlapping neurons, and finally deconvolves the fluorescence signal to produce probability amplitudes for the existence of spikes. The method involves constrained non-negative matrix factorization of fluorescence into time and space components, and finally an autoregressive deconvolution process for determining the (denoised) calcium transient and the spike probability amplitudes. In our work, the autoregressive model used is a two-step autoregressive model AR(2).

Thresholding We use raw fluorescence minus the background to find the "noise intervals", which are the frames where the aforementioned fluorescence has negative values. The deconvolved signal restricted on the noise intervals is called S_{noise}. In the case of S_{noise} with more than 3 nonzero values, we evaluate the 68th percentile of the nonzero noise values distribution. This is meant to give the scale of the noise, and multiples of this are used as thresholds for determining spikes (indicated as *dc* thresholds). Note that the 68th percentile corresponds to the standard deviation in the normal distribution. The 68th percentile is used, instead of evaluating the standard deviation, to avoid an increase in the standard deviation due to outlier values. We found that spike determination is not very sensitive to threshold variations if we choose the threshold to be 1.5*(68th percentile of noise). In the case of S_{noise} with 3 or less non-zero values (> 0.001), all S_{noise} 's nonzero values become 0s and the rest 1s. This is justified by the fact that although there are noise intervals long enough, there are too few nonzero S_{noise} frames, suggesting that for these neurons there is very little noise. Note that less than or equal to 3 non-zero values for S_{noise} are not sufficient to permit characterization of noise (evaluation of 68th percentile of noise). This can be further tested by comparing the distributions of the firing rates of two neuronal populations, namely the one with S_{noise} of 3 or less non-zero values (red histogram), and the remaining ones. For the second population, the noise standard deviation has been estimated through the 68th percentile of S_{noise} (gray histogram). For these neurons, the cutoff has been taken to be 1.5*(68th percentile of noise).

Functional Connectivity Analysis Methods

STTC To quantify functional connectivity, it is important to use a robust temporal correlation measure. Here, we use the spike time tiling coefficient (STTC), introduced by Cutts and Eglen[16], which performs favorably against 33 other commonly-used measures and is less sensitive to firing rate.
The STTC of neuron A relative to B is defined as:

$$STTC(\Delta t) = \frac{1}{2}\left(\frac{P_A - T_B}{1 - P_A T_B} + \frac{P_B - T_A}{1 - P_B T_A}\right),$$

where P_A is the proportion of firing events of neuron A found within an interval ($\pm\Delta$t) around each firing event of neuron B, T_B is the proportion of the recording duration that falls within an interval ($\pm\Delta$t) around each firing event of neuron B, and likewise for T_A and P_B. STTC has been symmetrized and normalized to lie within [-1, 1]. The bulk of the results presented below use STTC values measured at Δt=0, i.e., the probability that neurons fire in synchrony within one calcium imaging frame, for which the two measures are identical. Since the calcium frames last 155ms in our experiments, the order of events with a temporal difference less than that cannot be distinguished, so the temporal synchrony correlation STTC measure we compute is insensitive to temporal differences smaller than 155ms. We also computed STTCs by taking Δt= 300ms (i.e. broadening the window of synchrony to 2 additional imaging frames; Suppl. Fig. 2.1.A-B), in which case we used an extension of the STTC measure we devised to take into consideration the temporal order of occurrence of spikes in A relative to B, i.e. reflect the probability that spikes of one neuron may systematically precede (or follow) spikes of the other.

Estimation of the null in STTC To evaluate the extent to which the observed STTC values could arise by sequences with the same number of firing events and inter-event intervals but without any temporal structure, we circularly shifted the firing events of each neuron by a uniformly sampled integer number of imaging frames within the interval 500 times independently. From these iterations, we obtained a null distribution of STTC values for each pair of neurons. The *z-score of each edge between neurons* is defined as: $z_{score} = \dfrac{STTC - m_{null}}{\sigma_{null}}$, where the m_{null} and σ_{null} correspond to the mean and standard deviation of the null distribution, respectively. The z-score quantifies the distance of the observed STTC value from the mean of the null STTC distribution in units of standard deviations of the null STTC distribution.

Statistically significant of the STTC in each Layer We identify the positive inter-neuronal functional correlations ("edges") with z-score > 4 in each layer, considering neurons located at the same layer (L2, L3, and L4). In the histograms, we merge the L2 and L3 distributions (union of edges), and report it as L2/3. Thus, L2/3 includes only *intra-layer* edges, between pyramidal neurons that belong at the same layer. Similarly, we compute the negative inter-neuronal functional connections at different z-score levels.

Functional Connectivity and Bias in Tuning Function We compute the bias in tuning function, by considering all neuronal pairs in a specific layer case (e.g., intra-layer L4 or L2/3 or inter-layer from L4 to L2/3). For those neuronal pairs, we estimate the percentage of statistically significant edges (z-score > 4) that have absolute orientation difference within a certain interval (bin) PSE(bin). Similarly, for the aforementioned neuronal pairs, we form the null, which is the set of functional connections edges with z-score in [-2, 2] and identify the percentage of them that belong in that bin (i.e., Null(bin)). We then report the difference computed in each bin normalized by the probability of the null in that bin ($\frac{PSE(bin) - Null(bin)}{Null(bin)}$).
Estimation of the probability of firing of a recipient neuron The probability of firing of a recipient L2/3 neuron as a function of the number of its incoming functionally connected L4 neurons that fire simultaneously during a frame is shown in Fig. 5A, with bins (at the x-axis) for each number of cofiring events. To profile the probability of firing of the putative recipient L2/3 neurons, we then apply weighted linear regression on these data points, as well as a weighted ReLU fit. To improve the reliability of regression, we first merged the original bins to ensure that each bin has a sufficient number of frames (here at least 10 frames) as follows: For each recipient neuron, we start from the rightmost (largest) bin (i.e., [N, N+1)), where N is the maximum number of cofiring events of its incoming functionally connected L4 neurons, and iteratively "scan" the bins from right to left merging bins to ensure that each merged bin has at least 10 frames. We only merge consecutive bins as follows: **1)** examine the number of frames at the current bin and if it has less than 10 frames, **2)** merge it to the next bin at the left (creating a "super-bin"). If the newly-merged bins (super-bin) has still less than 10 frames, we continue

the bin-merging: merge the super-bin with the next bin at the left until we the set of consecutive bins (super-bins) contain *at least 10 frames*. We then continue with the scanning as described above with the next bin. The center of the merged bins corresponds to the (rounded) weighted average of the original bins, with *weights based on their number of frames*. For each recipient neuron, we perform *weighted linear fitting and weighted ReLU fitting* on its data points, of the form (cofiring events, firing probability), for co-firing events in the range of [0, N]. The weight of the i-th point (bin) is based on the standard error of the mean in that bin (normalized by the maximum standard error of the mean (SEM) observed in that recipient neuron, across all its points). In the case of the percent of cofiring events, the bins used are of the form [0, 0.5), [0.5, 1.5), . . . , [99.5, 100] percent of cofiring events.
Estimation of the Control Input Neuronal Group of a Putative Recipient Neuron We randomly select neurons of the same layer and of *equal size as the observed input neuronal group of interest* that does *not* overlap with it.

Weighted ReLU fitting For each recipient neuron, the weighted ReLU fitting is performed on the points (x, y) (namely, the number of cofiring events of the neurons of the STTC group and the firing probability of the recipient neuron, respectively) after bin merging, for cofiring events in the range [0, N], where N is the maximum number of cofiring events of the STTC group of the recipient neuron. Each point is weighted based on the standard error of the mean of the firing probability in the corresponding bin and normalized by the maximum standard error of the mean observed across bins of that recipient neuron The ReLU fit is composed of two parts, namely a constant/fixed part (parameterized by the plateau intercept and the plateau length) and a linearly increasing one (parameterized by the slope and the line intercept). The plateau intercept is the intersection point of the horizontal part with the y-axis. The plateau length is the point in the x-axis where the horizontal part stops and the linear part begins. The value for the line intercept is estimated from the values of the other parameters, to maintain continuity. The other three parameters are estimated using a subspace bounded implementation of the least squares algorithm, so that the parameters are restricted in specific value ranges.

Weighted Linear Regression For each recipient neuron, the weighted linear regression is performed on the points (x, y), namely, the number of cofiring events of the neurons of the STTC group and the firing probability of the recipient neuron, respectively, after bin merging, for cofiring events in the range [0, N], where N is the maximum number of cofiring events of the STTC group of the recipient neuron. Each point is weighted based on the standard error of the mean of the firing probability in the corresponding bin and normalized by the maximum standard error of the mean observed across bins of that recipient neuron. The slope and the intercept of the linear fit are then estimated using the weighted least squares algorithm.

R2 The coefficient of determination is the proportion of the variation in the dependent variable that is predictable from the independent variable(s). It provides a measure of how well observed outcomes are replicated by the model.

Unweighted:

$$SSE = \sum_{i}^{n} (y_i - \hat{y}_i)^2, \qquad SST = \sum_{i}^{n} (y_i - \bar{y})^2, \qquad R^2 = 1 - \frac{SSE}{SST},$$

where SSE is the sum of squares of residuals, SST is the total sum of squares, i is the i-th element, $\hat{y}_i$ is the model's prediction for the i-th element, y_i is the observed value for the i-th element, and $\bar{y}$ is the mean observed value.

Weighted:

$$SSE_{weighted} = \sum_{i}^{n} w_i (y_i - \hat{y}_i)^2, \qquad SST_{weighted} = \sum_{i}^{n} w_i (y_i - \overline{y_{weighted}})^2, \qquad R^2_{weighted} = 1 - \frac{SSE_{weighted}}{SST_{weighted}},$$

where $SSE_{weighted}$ is the sum of weighted squares of residuals, $SST_{weighted}$ is the total sum of weighted squares, i is the i-th element, $\hat{y}_i$ is the model's prediction for the i-th element, y_i is the observed value for the i-th element, w_i is the weight assigned to the i-th element, and $\overline{y_{weighted}}$ is the weighted mean of the observed values.

RMSE The root-mean-square error (RMSE) is a measure of the differences between values (sample or population

values) predicted by a model or an estimator and the values observed and is therefore a measure of the model's accuracy.

Unweighted:

$$RMSE = \sqrt{\frac{\sum_i^N (y_i - \hat{y}_i)^2}{N}} \ ,$$

where i is the i-th element, $\hat{y}_i$ is the model's prediction for the i-th element, y_i is the observed value for the i-th element, and N is the total number of elements.

Weighted:

$$RMSE = \sqrt{\frac{\sum_i^N w_i (y_i - \hat{y}_i)^2}{\sum_i^N w_i}} \ ,$$

where i is the i-th element, $\hat{y}_i$ is the model's prediction for the i-th element, y_i is the observed value for the i-th element, w_i is the weight assigned to the i-th element, and N is the total number of elements.

Normalized Root-Mean-Square Error (NRMSE) The normalized root-mean-square error (NRMSE) is equal to the RMSE normalized by the value range of the values observed. It is a metric used for comparing models with different scales.

$$NRMSE = \frac{RMSE}{y_{max} - y_{min}}$$

where $RMSE$ is the root-mean-square error, y_{max} is the maximum observed value, and y_{min} is the minimum observed value. The $RMSE$ used can be either weighted or unweighted.

Statistical Tests and Statistical Significance All histograms report statistics that indicate the sample mean and standard deviation of the sample means across mice (n=5), while the error bars indicate the SEM across mice for each specific bin. For all histograms, the statistical tests used are the permutation of means, the Welch's t-test and the ANOVA (F-test) and the statistical significance reported results from the statistical test with the highest p-value (in order to be more conservative). For example, for the comparison of the observed vs. null for a specific metric, the means of the observed and the null are calculated per mouse, and then using the 5 means from each distribution, the above statistical tests are performed across mice. For each panel, the level at which the significance test was rejected is shown in the plots using the following notation: empty or "n.s.", if the null hypothesis of equal means is not rejected (p-value > 0.05); "*", if the null hypothesis is rejected for a significance level of 0.05 (p-value < 0.05); "**", if the null hypothesis is rejected for a significance level of 0.01 (p-value < 0.01); and "***", if the null hypothesis is rejected for a significance level of 0.001 (p-value < 0.001).

Graph-theoretical Metrics

Degree of Connectivity and Clustering Coefficient For each neuron, we estimate the ratio of the neurons with statistically significant functional connections (z-score > 4), i.e., 1FC neighbors, per layer case, which corresponds to the *normalized* degree of connectivity in that layer. For example, a L4 neuron has an intra-layer degree of connectivity of 0.1 if that neuron is functionally connected with the 10% of the L4 neuronal population. Moreover, we estimate the ratio of neuronal pairs of its 1FC neighbors that form statistically significant functional connections with each other, considering *only* the frames at which the index neuron does not fire, to account for possible bias. This corresponds to the clustering coefficient of the neuron. For example, an L2/3 neuron with a L4→L2/3 clustering coefficient of 10% indicates that exactly 10% of all possible pairwise functional connections between its L4 neighbors are statistically significant.

Small-worldness A network is characterized as small-world-like when it has short paths between nodes and high

clustering. In order to quantify the degree to which the observed networks exhibit small-world characteristics, we compare the average shortest path length and the clustering coefficient of the observed graphs to those of theoretical graphs[52,58]. The observed functional networks were formed considering all neurons within the layer of interest and their statistically significant functional connections (STTC z-score > 4). Each theoretical graph was constructed using the same number of neurons as their corresponding observed functional network.

For the **Erdős–Rényi** networks, $ER(N, p)$, where N is the total number of neurons in the layer of interest and p the probability that two neurons are functionally connected (equal to the mean normalized degree of the respective biological network), we placed an edge between each pair of neurons with probability p.

The **regular ring** graphs were created by assigning a fixed degree of connectivity to each of the N nodes. Specifically, the nodes are placed on the "ring", in a circular topology and each node has a degree of connectivity equal to $2k$, with k connections to its k nearest neighbors on its left and k connections with its nearest neighbors on its right. We then compare the three graphs concerning the shortest paths between pairs of neurons and the clustering coefficient.

Small World Index Another way to assess the small-worldness of a network is the Small World Index (SWI), a value between 0 and 1 which is higher for small-worldly graphs, which is defined as follows :

$$\text{SWI} = \frac{L - L_l}{L_r - L_l} \times \frac{C - C_r}{C_l - C_r}$$

where C is the clustering coefficient, L is the path length, and l,r correspond to regular-ring and random graphs respectively.

Network Robustness The networks of the layers L4 and L2/3 are **robust** given the presence of a *giant component* that includes almost the entire neuronal population recorded at each corresponding layer. Note that a giant component is a sub-network that contains a large number of neurons (of the original network) and their functional connections. L4 contains a giant component that persists under high z-score thresholds used to determine the statistically significant connections (up to 8) and includes approximately 80% of its neuronal population (as demonstrated in Suppl. Fig. 4.9A). L2/3 follows a similar trend but up to a smaller z-score value. Similar results are obtained when we employ the Molloy-Reed criterion, derived for a particular family of random graphs with a specific distribution of normalized degrees of connectivity[55,56], to examine the robustness of the functional networks[52]. According to the "Molloy-Reed"-based network robustness index, calculated as the ratio of the second moment of the degree of connectivity over the mean degree of connectivity[52,55,56], the functional connectivity of these layers exhibits significant robustness (well above 2) larger than their corresponding Erdős–Rényi and regular ring graphs (Suppl. Figures 4.9, and methods for the criterion). Interestingly, even for very high z-score thresholds, the resulting functional networks at both layers remain well-connected. It is part of our future work to assess the robustness using also other techniques based on the removal of targeted functional connections and neurons.

Network Robustness: Molloy-Reed Criterion The Molloy-Reed criterion $\kappa = \langle k^2 \rangle / \langle k \rangle > 2$[55,56] links the network's integrity, as expressed by the presence or the absence of a giant component, to the mean degree of connectivity:

$$\langle k \rangle = \frac{1}{n} \sum_{i=1}^{n} d_i$$

and its second moment:

$$\langle k^2 \rangle = \frac{1}{n} \sum_{i=1}^{n} d_i^2,$$

where d_i is the degree of connectivity of node i and n is the total number of nodes in the network. It is valid for any degree distribution p_k[52] (Chapter 8). In general, a network displays enhanced robustness, if its breakdown threshold (directly depending on κ) deviates from the random network prediction. The very high κ and high mean clustering coefficient, especially in L4 but also L2/3, significantly higher than the corresponding Erdős–Rényi graphs, suggest enhanced robustness (see Suppl. Figure 4.8, 4.9). In general, real networks are robust to random failures but fragile to targeted attacks.

Peer Identification of L2/3 Neurons

To identify the L2/3 group of peers of an L2/3 neuron, we assess which L2/3 neurons are strongly modulated by the L4-1FC group of the neuron. Specifically, for each L2/3 neuron (say neuron R), another L2/3 neuron (e.g., neuron P) is a *peer*, if P becomes modulated by the L4 STTC group of R. For that, we employ the event triggered average (ETA) of P with respect to the L4-1FC group cofiring of R. We first identify the peak of the ETA of neuron P (say at lag l) and examine whether it is statistically significantly different (above z-score threshold 4) from the baseline signal of the L4-1FC group cofiring. A neuron P with firing that is modulated by the L4-1FC group of R is named L2/3 peer of R.

Reliability of the Activity Transmission from an L4-1FC Group to L2/3-1FC Group using Sensitivity, Specificity, and Precision Let's say that the L4 and L2/3 1FC groups are *active* when there is a *significantly large cofiring* (at z-score>3 for L4 and z-score>2 for L2/3). The activity transmission manifests at frames when *both groups are simultaneously active*. We demonstrate that the group-to-group transmission is more reliable than the group-to-neuron as measured by the sensitivity, specificity, accuracy and precision that compare the synchronicity of the activity of the L4-1FC group with the activity of the corresponding L2/3-1FC vs. the firing of the L2/3 neuron. The sensitivity measures the fraction of frames at which the L2/3-1FC group is active that the L4-1FC group is also active, while the specificity corresponds to the fraction of frames at which the L2/3-1FC group is inactive that the L4-1FC group is also inactive. The accuracy computes the fraction of frames where the L4 and L2/3 groups are either both active or both inactive. The precision computes the fraction of frames at which the L4-1FC group is active that the L2/3-1FC group is also active. Thus we have

$$Sensitivity = \frac{|A_{L4} \cap A_{L2/3}|}{|A_{L2/3}|}$$

$$Specificity = \frac{|I_{L4} \cap I_{L2/3}|}{|I_{L2/3}|}$$

$$Accuracy = \frac{|A_{L4} \cap A_{L2/3}| + |I_{L4} \cap I_{L2/3}|}{|F|}$$

$$Precision = \frac{|A_{L4} \cap A_{L2/3}|}{|A_{L2/3}|}$$

Where A_{L4} and $A_{L2/3}$ are the sets containing the indices of the active 2-photon frames for the L4 and L2/3 1FC groups respectively, I_{L4} and $I_{L2/3}$ are the corresponding sets for the inactive frames and F is the set containing all the recorded frames of the one hour period.

Normalization process on the L4-1FC group cofiring for the prediction of the L2/3 neuronal response

In studying the response properties of L2/3 neurons with respect to their Layer4 STTC group, we searched for a normalization by a power of the group size, to have similar response curves irrespective of the group size. First of all, it is *not* at all obvious that such a normalization exists *over a wide range of group sizes*. Second, the input statistics depend on the group size, unless neurons fire independently and the input is normalized by the square root of the group size. Hence, if the input is normalized in such a way, the L2/3 neuronal response corresponds to the probability of the normalized input, hence the L2/3 neuron will know how rare cofirings are **irrespective of group size**. To conclude, one way to make the L2/3 neuron to respond according to the rareness of a cofiring, is *through the normalization of the input by the square root of the group size.* Below we present a simple theoretical model to show this normalization and provide an intuition:

Let's suppose for simplicity that the L4 connectivity group consists of N independent neurons firing each with probability p within one frame. In this case, the mean firing is $\mu = Np$ and the firing standard deviation is $\sigma = \sqrt{(Np(1-p))}$. If we denote by F the L4 connectivity group firing random variable, then, by the central limit theorem, we have

$$P\left(f \leq \frac{(F - Np)}{\sqrt{N}} \leq f + \delta f\right) \approx \frac{1}{\sqrt{2\pi p(1-p)}} e^{-\frac{f^2}{2p(1-p)}} \delta f$$

. What is important about this distribution is that it is *independent of N*. Hence if L2/3 neurons have response probability proportional to the normalized group firing above the mean, $p_R = a((F - Np)/\sqrt{N}) + b$, for the same constants a, b, they would respond under the same distribution *irrespective of the size of their L4 group*, permitting a more homogeneous response in L2/3. In this case, the slope of the L2/3 neuron response against their L4-1FC group cofiring normalized by $N^{1/2}$ would be the same irrespective of the L4-1FC group size. This is slightly less than the $0.6 - 0.7$ found experimentally. This difference might be attributed to either the existence of correlations between L4 neurons or differences in the probability of firing between different neurons in L4.

Acknowledgments

We would like to thank the members of Tolias Lab at the Department of Neuroscience at Baylor College of Medicine in Houston, TX for performing the two-photon (mesoscope) experiments, sharing the datasets to us, and providing valuable feedback about the data. We are also grateful to Vassilis Sideridis and Nikolaos Ntorvas who contributed significantly to the implementation of several aspects of the preliminary analysis. Several student interns at FORTH as part of their training, their B.Sc. Thesis or FORTH research assistanship, were involved in this project by implementing or validating different parts of the preliminary analysis, namely, Andreas Sapoutzis, Ioannis Siriopoulos, Ioannis Fotis, Orestis Mousouros, Maria Plakia, Ioannis Charalambakis, Andreas Karambasis, Christos Mamoudis, Kostantinos Kokolakis, Charalampos Peteinarelis, Theodora Sambalou, Nikolaos Tzanakis, and Emmanouel Patronakis. Finally, we would like to thank Dr. Georgios Keliris (FORTH) for reviewing the paper and providing comments.

This work has received funding from the European Union's Horizon 2020 research and innovation program under the Marie Skłodowska-Curie grant agreement No 101007926 and from the Hellenic Foundation Research Institute (HFRI), the neuron-AD project number 04058 and neuronXnet project number 2285 (PI: Maria Papadopouli). This research was also supported by R01 NS113890, and R21 NS127299 (PI: Stelios Smirnakis).

Code Availability

The code and additional information about the algorithms will be released during the peer review process. We will also release the code/algorithm as soon as the manuscript is published at a neuroscience journal (in github).

References

1. De Lorente, N. R. Cerebral cortex: architecture, intracortical connections, motor projections. *Physiology of the nervous system,* 288–330 (1949).
2. Abeles, M., Bergman, H., Margalit, E. & Vaadia, E. Spatiotemporal firing patterns in the frontal cortex of behaving monkeys. *Journal of Neurophysiology* **70,** 1629–1638. https://doi.org/10.1152/jn.1993.70.4.1629 (Oct. 1993).
3. Hebb, D. O. The first stage of perception: growth of the assembly. *The Organization of Behavior* **4,** 78–60 (1949).
4. Carrillo-Reid, L., Yang, W., Bando, Y., Peterka, D. S. & Yuste, R. Imprinting and recalling cortical ensembles. *Science* **353,** 691–694. https://doi.org/10.1126/science.aaf7560 (Aug. 2016).
5. Panzeri, S., Moroni, M., Safaai, H. & Harvey, C. D. The structures and functions of correlations in neural population codes. *Nature Reviews Neuroscience* **23** (2022).
6. Averbeck, B. B., Latham, P. E. & Pouget, A. Neural correlations, population coding and computation. *Nature reviews neuroscience* **7** (2006).
7. Yuste, R. From the neuron doctrine to neural networks. *Nature Reviews Neuroscience.* https://doi.org/10.1038/nrn3962 (2015).
8. Cossart, R., Aronov, D. & Yuste, R. Attractor dynamics of network UP states in the neocortex. *Nature* **423,** 283–288. ISSN: 1476-4687. http://dx.doi.org/10.1038/nature01614 (May 2003).
9. Miller, J.-e. K., Ayzenshtat, I., Carrillo-Reid, L. & Yuste, R. Visual stimuli recruit intrinsically generated cortical ensembles. *Proceedings of the National Academy of Sciences of the United States of America* **111,** E4053–61. ISSN: 0027-8424. https://europepmc.org/articles/PMC4183303 (Sept. 2014).
10. Russo, E. & Durstewitz, D. Cell assemblies at multiple time scales with arbitrary lag constellations. *Elife* **6,** e19428 (2017).

11. Yuste, R., Cossart, R. & Yaksi, E. Neuronal ensembles: Building blocks of neural circuits. *Neuron.* ISSN: 0896-6273. https://www.sciencedirect.com/science/article/pii/S0896627323009674 (2024).
12. Smyrnakis, I. & Smirnakis, S. Information Transfer Through Stochastic Transmission of a Linear Combination of Rates. *Neural Computation* **25,** 2265–2302. ISSN: 0899-7667 (Sept. 2013).
13. Kenet, T., Bibitchkov, D., Tsodyks, M., Grinvald, A. & Arieli, A. Spontaneously emerging cortical representations of visual attributes. *Nature* **425** (2003).
14. Luczak, A., Barthó, P. & Harris, K. D. Spontaneous Events Outline the Realm of Possible Sensory Responses in Neocortical Populations. *Neuron* **62,** 413–425. https://doi.org/10.1016/j.neuron.2009.03.014 (May 2009).
15. Palagina, G., Meyer, J. F. & Smirnakis, S. M. Inhibitory units: an organizing nidus for feature-selective subnetworks in area V1. *Journal of Neuroscience* **39** (2019).
16. Cutts, C. S. & Eglen, S. J. Detecting pairwise correlations in spike trains: an objective comparison of methods and application to the study of retinal waves. *Journal of Neuroscience* **34** (2014).
17. Fornito, A., Zalesky, A. & Breakspear, M. The connectomics of brain disorders. *Nature Reviews Neuroscience* **16,** 159–172 (2015).
18. Stam, C. J. Modern network science of neurological disorders. *Nature Reviews Neuroscience* **15,** 683–695 (2014).
19. Pnevmatikakis, E. A., Soudry, D., Gao, Y., Machado, T. A., Merel, J., Pfau, D., Reardon, T., Mu, Y., Lacefield, C., Yang, W., *et al.* Simultaneous denoising, deconvolution, and demixing of calcium imaging data. *Neuron* **89** (2016).
20. Senzai, Y., Fernandez-Ruiz, A. & Buzsáki, G. Layer-specific physiological features and interlaminar interactions in the primary visual cortex of the mouse. *Neuron* **101** (2019).
21. Pnevmatikakis, E. A., Soudry, D., Gao, Y., Machado, T. A., Merel, J., Pfau, D., Reardon, T., Mu, Y., Lacefield, C., Yang, W., Ahrens, M., Bruno, R., Jessell, T. M., Peterka, D. S., Yuste, R. & Paninski, L. Simultaneous Denoising, Deconvolution, and Demixing of Calcium Imaging Data. *Neuron* **89,** 285–299. https://doi.org/10.1016/j.neuron.2015.11.037 (Jan. 2016).
22. Froudarakis, E., Berens, P. & Ecker, A. Population code in mouse V1 facilitates readout of natural scenes through increased sparseness. *Nature Neuroscience* (2014).
23. Stringer, C., Pachitariu, M., Steinmetz, N., Carandini, M. & Harris, K. D. High-dimensional geometry of population responses in visual cortex. *Nature* **571** (2019).
24. Kohn, A., Zandvakili, A. & Smith, M. A. Correlations and brain states: from electrophysiology to functional imaging. *Current Opinion in Neurobiology,* 434–438 (2009).
25. Cohen, M. & Kohn, A. Measuring and interpreting neuronal correlations. *Nature Neuroscience* **14,** 811–819 (2011).
26. Bair, W., Zohary, E. & Newsome, W. T. Correlated Firing in Macaque Visual Area MT: Time Scales and Relationship to Behavior. *Journal of Neuroscience* **21,** 1676–1697 (2001).
27. Ecker, A. S., Berens, P., Keliris, G. A., Bethge, M., Logothetis, N. K. & Tolias, A. S. Decorrelated Neuronal Firing in Cortical Microcircuits. *Science* **327,** 584–587 (2010).
28. Golshani, P., Gonçalves, J. T., Khoshkhoo, S., Mostany, R., Smirnakis, S. & Portera-Cailliau, C. Internally mediated developmental desynchronization of neocortical network activity. *Journal of Neuroscience* **29,** 10890–10899 (2009).
29. Ch'Ng, Y. & Reid, C. Cellular Imaging of Visual Cortex Reveals the Spatial and Functional Organization of Spontaneous Activity. *Frontiers in Integrative Neuroscience* (2010).
30. Li, B., Chavarha, M., Kobayashi, Y., Yoshinaga, S., Nakajima, K., Lin, M. Z. & Inoue, T. Two-photon voltage imaging of spontaneous activity from multiple neurons reveals network activity in brain tissue. *Iscience* **23** (2020).
31. Cossell, L., Iacaruso, M., Muir, D., Houlton, R., Sader, E. N., Ko, H., Hofer, S. B. & Mrsic-Flogel, T. D. Functional organization of excitatory synaptic strength in primary visual cortex. *Nature* **518** (2015).
32. Ecker, A. S., Berens, P., Keliris, G. A., Bethge, M., Logothetis, N. K. & Tolias, A. S. Decorrelated Neuronal Firing in Cortical Microcircuits. *Science* **327,** 584–587. https://doi.org/10.1126/science.1179867 (Jan. 2010).
33. Ko, H., Hofer, S. B., Pichler, B., Buchanan, K. A., Sjöström, P. J. & Mrsic-Flogel, T. D. Functional specificity of local synaptic connections in neocortical networks. *Nature* **473,** 87–91 (2011).
34. Lee, W.-C. A., Bonin, V., Reed, M., Graham, B. J., Hood, G., Glattfelder, K. & Reid, R. C. Anatomy and function of an excitatory network in the visual cortex. *Nature* **532,** 370–374 (2016).

35. Das, A. & Gilbert, C. D. Topography of contextual modulations mediated by short-range interactions in primary visual cortex. *Nature* **399,** 655–661 (1999).
36. De Vries, S. E., Lecoq, J. A., Buice, M. A., Groblewski, P. A., Ocker, G. K., Oliver, M., Feng, D., Cain, N., Ledochowitsch, P., Millman, D., *et al.* A large-scale standardized physiological survey reveals functional organization of the mouse visual cortex. *Nature neuroscience* **23,** 138–151 (2020).
37. Fahey, P. G., Muhammad, T., Smith, C., Froudarakis, E., Cobos, E., Fu, J., Walker, E. Y., Yatsenko, D., Sinz, F. H., Reimer, J., *et al.* A global map of orientation tuning in mouse visual cortex. *BioRXiv* (2019).
38. Olaf Sporns, C. J. H. & Kötter, R. Identification and Classification of Hubs in Brain Networks. *Plos One* (2007).
39. Bonifazi, P., Goldin, M., Picardo, M. A., Jorquera, I., Cattani, A., Bianconi, G., Represa, A., Ben-Ari, Y. & Cossart, R. GABAergic Hub Neurons Orchestrate Synchrony in Developing Hippocampal Networks. *Science* (2009).
40. Shadlen, M. N. & Newsome, W. T. The variable discharge of cortical neurons: implications for connectivity, computation, and information coding. *Journal of neuroscience* **18** (1998).
41. Sato, T. K., Haider, B., Häusser, M. & Carandini, M. An excitatory basis for divisive normalization in visual cortex. *Nature neuroscience* **19,** 568–570 (2016).
42. Vinck, M., Batista-Brito, R., Knoblich, U. & Cardin, J. A. Arousal and Locomotion Make Distinct Contributions to Cortical Activity Patterns and Visual Encoding. *Neuron* **86,** 740–754. ISSN: 0896-6273. https://www.sciencedirect.com/science/article/pii/S0896627315002524 (2015).
43. Polack, P.-O., Friedman, J. & Golshani, P. Cellular mechanisms of brain state–dependent gain modulation in visual cortex. *Nature Neuroscience* **16,** 1331–1339. https://doi.org/10.1038/nn.3464 (July 2013).
44. Okun, M., Yger, P., Marguet, S. L., Gerard-Mercier, F., Benucci, A., Katzner, S., Busse, L., Carandini, M. & Harris, K. D. Population rate dynamics and multineuron firing patterns in sensory cortex. *Journal of Neuroscience* **32** (2012).
45. Barlow, H. B. Adaption and decorrelation in the cortex. *The computing neuron* (1989).
46. Kohn, A., Coen-Cagli, R., Kanitscheider, I. & Pouget, A. Correlations and neuronal population information. *Annual review of neuroscience* **39** (2016).
47. Shadlen, M. N. & Newsome, W. T. The Variable Discharge of Cortical Neurons: Implications for Connectivity, Computation, and Information Coding. *The Journal of Neuroscience* **18,** 3870–3896. https://doi.org/10.1523/jneurosci.18-10-03870.1998 (May 1998).
48. Meyer, J. F., Golshani, P. & Smirnakis, S. M. The effect of single pyramidal neuron firing within layer 2/3 and layer 4 in mouse v1. *Frontiers in Neural Circuits* **12,** 29 (2018).
49. Kwan, A. C. & Dan, Y. Dissection of cortical microcircuits by single-neuron stimulation in vivo. *Current Biology* **22,** 1459–1467 (2012).
50. Smyrnakis, I., Papadopouli, M., Pallagina, G. & Smirnakis, S. Information capacity of a stochastically responding neuron assembly. *Neurocomputing* **436,** 22–34. https://doi.org/10.1016/j.neucom.2020.12.130 (May 2021).
51. Braitenberg, V. & Schüz, A. *Cortex: statistics and geometry of neuronal connectivity* (Springer Science & Business Media, 2013).
52. Barabasi. *Network Science* https://doi.org/10.1098/rsta.2012.0375 (Cambridge University Press, 2015).
53. Cohen, H. *Complex Networks: Structure, Robustness and Function* https://doi.org/10.1017/CBO9780511780356 (Cambridge University Press, 2010).
54. Newman, M. E. The structure and function of complex networks. *SIAM review* **45,** 167–256 (2003).
55. Molloy, M. & Reed, B. A critical point for random graphs with a given degree sequence. *Random structures & algorithms* **6,** 161–180 (1995).
56. Molloy, M. & Reed, B. The size of the giant component of a random graph with a given degree sequence. *Combinatorics, probability and computing* **7,** 295–305 (1998).
57. Bassett, D. S. & Bullmore, E. T. Small-World Brain Networks Revisited. *The Neuroscientist* **23.** PMID: 27655008, 499–516. eprint: https://doi.org/10.1177/1073858416667720. https://doi.org/10.1177/1073858416667720 (2017).
58. Sporns, O. *Networks of the Brain* (MIT press, 2016).
59. Sporns, O. & Zwi, J. D. The Small World of the Cerebral Cortex. *Neuroinformatics* **2** (2004).

60. Reimer, J., Froudarakis, E., Cadwell, C. R., Yatsenko, D., Denfield, G. H. & Tolias, A. S. Pupil Fluctuations Track Fast Switching of Cortical States during Quiet Wakefulness. *Neuron* **84,** 355–362. https://doi.org/10.1016/j.neuron.2014.09.033 (Oct. 2014).
61. LeCun, Y., Bengio, Y. & Hinton, G. Deep learning. *nature* **521,** 436–444 (2015).
62. Ramachandran, P., Zoph, B. & Le, Q. V. Searching for activation functions. *arXiv preprint arXiv:1710.05941* (2017).
63. Nwankpa, C., Ijomah, W., Gachagan, A. & Marshall, S. *Activation Functions: Comparison of trends in Practice and Research for Deep Learning* 2018. arXiv: 1811.03378 [cs.LG].
64. Glorot, X., Bordes, A. & Bengio, Y. *Deep Sparse Rectifier Neural Networks* in *Proceedings of the Fourteenth International Conference on Artificial Intelligence and Statistics* (eds Gordon, G., Dunson, D. & Dudík, M.) **15** (PMLR, Fort Lauderdale, FL, USA, Nov. 2011), 315–323. https://proceedings.mlr.press/v15/glorot11a.html.
65. Carrillo-Reid, L. & Yuste, R. Playing the piano with the cortex: role of neuronal ensembles and pattern completion in perception and behavior. *Current Opinion in Neurobiology* (2020).
66. Carrillo-Reid, L., Miller, J.-e. K., Hamm, J. P., Jackson, J. & Yuste, R. Endogenous Sequential Cortical Activity Evoked by Visual Stimuli. *Journal of Neuroscience* **35** (June 2015).
67. Smyrnakis, I. & Smirnakis, S. Information Transfer Through Stochastic Transmission of a Linear Combination of Rates. *Neural Computation* **25,** 2265–2302 (2013).
68. Zhou, W., Bovik, A. C., Sheikh, H. R. & Simoncelli, E. P. Image Quality Assessment: From Error Visibility to Structural Similarity. *IEEE Transactions on Image Processing* (4 Apr. 2004).
69. Yatsenko, D., Reimer, J., Ecker, A. S., Walker, E. Y., Sinz, F., Berens, P., Hoenselaar, A., Cotton, R. J., Siapas, A. S. & Tolias, A. S. DataJoint: managing big scientific data using MATLAB or Python. http://dx.doi.org/10.1101/031658 (Nov. 2015).
70. Yatsenko, D., Walker, E. Y. & Tolias, A. S. *DataJoint: A Simpler Relational Data Model* 2018. https://arxiv.org/abs/1807.11104.
71. Paszke, A., Gross, S., Massa, F., Lerer, A., Bradbury, J., Chanan, G., Killeen, T., Lin, Z., Gimelshein, N., Antiga, L., Desmaison, A., Köpf, A., Yang, E., DeVito, Z., Raison, M., Tejani, A., Chilamkurthy, S., Steiner, B., Fang, L., Bai, J. & Chintala, S. in *Proceedings of the 33rd International Conference on Neural Information Processing Systems* (Curran Associates Inc., Red Hook, NY, USA, 2019).
72. Harris, C. R., Millman, K. J., van der Walt, S. J., Gommers, R., Virtanen, P., Cournapeau, D., Wieser, E., Taylor, J., Berg, S., Smith, N. J., Kern, R., Picus, M., Hoyer, S., van Kerkwijk, M. H., Brett, M., Haldane, A., del Río, J. F., Wiebe, M., Peterson, P., Gérard-Marchant, P., Sheppard, K., Reddy, T., Weckesser, W., Abbasi, H., Gohlke, C. & Oliphant, T. E. Array programming with NumPy. *Nature* **585,** 357–362. https://doi.org/10.1038/s41586-020-2649-2 (Sept. 2020).
73. Virtanen, P., Gommers, R., Oliphant, T. E., Haberland, M., Reddy, T., Cournapeau, D., Burovski, E., Peterson, P., Weckesser, W., Bright, J., van der Walt, S. J., Brett, M., Wilson, J., Millman, K. J., Mayorov, N., Nelson, A. R. J., Jones, E., Kern, R., Larson, E., Carey, C. J., Polat, İ., Feng, Y., Moore, E. W., VanderPlas, J., Laxalde, D., Perktold, J., Cimrman, R., Henriksen, I., Quintero, E. A., Harris, C. R., Archibald, A. M., Ribeiro, A. H., Pedregosa, F., van Mulbregt, P. & SciPy 1.0 Contributors. SciPy 1.0: Fundamental Algorithms for Scientific Computing in Python. *Nature Methods* **17,** 261–272 (2020).
74. Hunter, J. D. Matplotlib: A 2D graphics environment. *Computing in Science & Engineering* **9,** 90–95 (2007).
75. Pandas development team, T. *pandas-dev/pandas: Pandas* version latest. Feb. 2020. https://doi.org/10.5281/zenodo.3509134.
76. McKinney, W. *Data Structures for Statistical Computing in Python* in *Proceedings of the 9th Python in Science Conference* (eds van der Walt, S. & Millman, J.) (2010), 56–61.
77. Pedregosa, F., Varoquaux, G., Gramfort, A., Michel, V., Thirion, B., Grisel, O., Blondel, M., Prettenhofer, P., Weiss, R., Dubourg, V., Vanderplas, J., Passos, A., Cournapeau, D., Brucher, M., Perrot, M. & Duchesnay, E. Scikit-learn: Machine Learning in Python. *Journal of Machine Learning Research* **12,** 2825–2830 (2011).